POLITECNICO DI TORINO
Repository ISTITUZIONALE

Techno-economic-environmental analysis of CO2 fermentation to acetic acid

Original
Techno-economic-environmental analysis of CO2 fermentation to acetic acid / Regis, F., Demichelis, F., Monteverde, A., Fino, D.. - In: CHEMICAL ENGINEERING JOURNAL. - ISSN 1385-8947. - 520:(2025), pp. 1-19. [10.1016/j.cej.2025.166138]

Availability:
This version is available at: 11583/3002308 since: 2025-08-03T10:26:13Z

Publisher:
Elsevier

Published
DOI:10.1016/j.cej.2025.166138

Terms of use:

This article is made available under terms and conditions as specified in the corresponding bibliographic description in the repository

Publisher copyright

(Article begins on next page)

18 November 2026

Chemical Engineering Journal 520 (2025) 166138



Contents lists available at ScienceDirect

Chemical Engineering Journal

journal homepage: www.elsevier.com/locate/cej



Techno-economic-environmental analysis of CO_2 fermentation to acetic acid

Francesco Regis [a,b,*], Francesca Demichelis [a], Alessandro Monteverde [a], Debora Fino [a,b,*]

[a] Department of Applied Science and Technology, Politecnico di Torino, Corso Duca degli Abruzzi 24, 10129 Turin, Italy
[b] Centre for Sustainable Future Technologies, Fondazione Istituto Italiano di Tecnologia, Via Livorno 60, 10144 Turin, Italy

ARTICLE INFO

Keywords:
CO_2 fermentation
Thermoanaerobacter kivui
Bio-acetic acid
Alkaline water electrolysis
Monoethanolamine absorption
LCA

ABSTRACT

Acetic acid, a key chemical in textiles, pharmaceuticals, and food industries, is largely produced via energy-intensive, fossil-based processes, driving greenhouse gas emissions. Gas fermentation using CO_2 and H_2 provides a sustainable alternative for bio-acetic acid production. The process, simulated on Aspen Plus®, targets the production of 37 kton.y^{-1} of glacial acetic acid (99.9 wt%). It includes an upstream phase to purify reactants, a fermentation stage, and a downstream step to concentrate the dilute culture broth into glacial acetic acid. H_2 is generated via alkaline water electrolysis, while CO_2 is captured using monoethanolamine absorption. The CO_2 originates from upgrading biogas into bio-methane, derived from anaerobic digestion of the organic fraction of municipal solid waste. Fermentation was modeled at 2 and 10 bar headspace pressures. Despite lower single-fermenter productivity, 2 bar operations reduced production costs and minimized formic acid formation, simplifying purification. The purification of acetic acid occurs with a hybrid process, which combines liquid-liquid extraction and azeotropic distillation using methyl tert-butyl ether as solvent, achieving 99.9 wt% purity. Economic analysis revealed an acetic acid production cost of 1.58 €.kg^{-1} for 37 kton.y^{-1} capacity, decreasing to 1.17 €.kg^{-1} at larger scales. With 2030 hydrogen cost projections, the acetic acid price could drop to 1.11 €.kg^{-1}, though remaining higher than the 2023 market price of 0.6 €.kg^{-1}. Environmental assessments proved that glacial bio-acetic acid production reached 47 % lower climate change impact, 73 % less fossil resource use, and 61 % reduced water consumption compared to traditional methods, confirming environmental benefits.

1. Introduction

Acetic acid (CH_3COOH), the second simplest aliphatic carboxylic acid, is widely used in textiles, pharmaceuticals, and the food industry. Key applications include vinyl acetate monomer for paints, adhesives, and textiles, terephthalic acid for PET resins and fibers, and acetic anhydride for cellulose-based products [1]. In 2022, the global acetic acid market reached $11.2 billion, with a projected 6.2 % annual growth, reaching $16.1 billion by 2028 [2].

Nowadays, most glacial acetic acid (GAA, >99.5 % purity) is produced from fossil fuels. The dominant method, methanol carbonylation, accounts for 75 % of production and reacts methanol (CH_3OH) with carbon monoxide (CO) at 150–200 °C and 30–50 bar [3]. Key processes include the rhodium-catalyzed Monsanto Process and the iridium-based Cativa Process by BP Chemicals [2]. Other methods include acetaldehyde oxidation, which oxidizes petroleum-derived acetaldehyde at ~150 °C and 55 bar with cobalt or chromium catalysts, and ethane partial oxidation using molybdenum-vanadium catalysts at 220–300 °C and 12–15 bar [4]. All these fossil-based methods are energy-intensive, emit greenhouse gases, involve costly catalysts, and generate waste and by-products, contributing to environmental pollution and requiring significant manpower and process safety measures [3].

Biological acetic acid production, known since ancient times, is widely used in the food industry for vinegar (4–12 % acetic acid). However, only 10 % of acetic acid world production is manufactured by bacterial fermentation to produce vinegar [5]. This method uses renewable carbon sources like fruits, honey, syrups, starch, beer, and wine to nourish bacteria. Ethanol, obtained from alcoholic fermentation of sugars, is then converted to acetic acid by bacteria belonging to two main species, *Acetobacter* and *Gluconacetobacter*, which oxidize ethanol to acetaldehyde and, ultimately, acetic acid in the presence of oxygen.

In recent years, biorefinery strategies for converting non-fossil sources into biofuels and chemical intermediates have gained

* Corresponding authors at: Department of Applied Science and Technology, Politecnico di Torino, Corso Duca degli Abruzzi 24, 10129 Turin, Italy.
E-mail addresses: francesco.regis@polito.it (F. Regis), debora.fino@polito.it (D. Fino).

https://doi.org/10.1016/j.cej.2025.166138
Received 15 March 2025; Received in revised form 9 July 2025; Accepted 16 July 2025
Available online 26 July 2025
1385-8947/© 2025 The Authors. Published by Elsevier B.V. This is an open access article under the CC BY license (http://creativecommons.org/licenses/by/4.0/).

Nomenclature

Parameters

A	Equipment cost attribute
CAPEX	Capital expenses, €
DR	Discount Rate, €
FCI	Fixed capital investment, €
IEC	Installed Equipment Cost, €
IT	Income Taxes, €
NPV	Net present value, €
OPEX	Operating expenses, €.y^{-1}
PEC	Purchase Equipment Cost, €
PL	Plant life, years
TAC	Total annualized costs, €
TAS	Total Annual Sales, €
TCI	Total Capital Investment, €
TEC	Total Equipment Cost, €
TIC	Total Installed Costs, €
TPC	Total Production Costs, €
TPI	Total Project Investment, €

Greek symbols

α_1	Installation labour factor
α_2	Building, material and labour factor
γ	Cost exponent factor
ΔT_{min}	Minimum temperature difference, °C

Acronyms and abbreviations

AEL	Alkaline electrolyser
APEA	Aspen Process Economic Analyzer
C	Column
CCSU	Carbon Capture Storage Utilization
CEPCI	Chemical Engineering Plant Cost Index
CSTR	Continuous stirred tank reactor
D	Decanter
E	Heat Exchanger
EHF	Enzymatic hydrolysis followed by fermentation
ELECNRTL	*Electrolyte non-random two Liquids*
ELECNRTL-RK	*Electrolyte non-random two Liquids with Ridley-Kwong Equation of State*
EPC	Engineering Procurement and Construction
F	Flash separator
FU	Functional units
GAA	Glacial acetic acid
GF	Gasification and subsequent syngas fermentation
GHG	Greenhouse gas
HEDP	Hybrid extraction/distillation process
KPI	Key Performance Indicator
LCA	Life Cycle Assessment
LCI	Life Cycle Inventory
MEA	Monoethanolamine
MPS	Medium Pressure Steam
MSP	Minimum Selling Price
MTBE	Methyl-tert-butyl ether
NRTL	*Non-random two Liquids*
NRTL –HOC	*Non-random two Liquids-Hayden O'Connel*
O&M	Operation and maintenance
OFMSW	Organic Fraction of Municipal Solid Waste
P	Pump
PEM	Proton Exchange Membrane
PFD	Process Flow Diagram
R	Reactor
S	Section
SOEC	Solid Oxide Water Electrolysis Cell

Subscripts

1	Reference year
2	Base year
t	Plant operating year

significant attention. This shift aims to reduce dependence on fossil fuels, lower GHG emissions, and meet global energy and chemical demands. Fermentation has emerged as a promising low-carbon option, enabling fuel production from biomass. However, it faces challenges. Second-generation biomass is preferred over first-generation to avoid disrupting food supply, but it requires costly pretreatment and hydrolysis to separate cellulose and hemicellulose from lignin and produce fermentable sugars [6]. Gas fermentation offers a viable alternative by gasifying biomass and using the resulting syngas as fermentation feedstock, maximizing biomass utilization, including lignin, for higher yields [7]. This flexible process accommodates diverse feedstocks, such as municipal solid and industrial waste, and operates at mild pressures and temperatures [8]. However, it suffers from low gas-liquid mass transfer rates and the high cost of biological media, as detailed by Gao et al., 2013 and Phillips et al., 2017 ([9,10]). Alternatively, gas fermentation can use CO_2 captured from industrial emissions or the atmosphere and H_2 produced via water electrolysis as feedstocks instead of syngas.

Acetogenic bacteria, such as *Thermoanaerobacter kivui*, can utilize the reductive Wood-Ljungdahl Pathway to convert carbon dioxide into acetic acid [11]. Thermophilic acetogens like *T. kivui* are particularly promising due to their lower contamination risk and higher metabolic efficiency [12]. These strictly anaerobic, Gram-negative bacteria can support both autotrophic and heterotrophic metabolism, growing on diverse organic substrates (e.g., hexoses, pentoses, alcohols, methyl groups, and formic acid) or inorganic substances like carbon monoxide (CO), carbon dioxide (CO_2), and hydrogen (H_2) [5]. Experimental tests by Regis et al., 2024 in a pressurized stirred-tank reactor optimized acetic acid production from H_2 and CO_2 using *T. kivui*, achieving peak cell-specific productivity at 10 bar with a 3:1 H_2:CO_2 ratio [13]. With an optimal growth temperature of 66 °C and pH 6.5, *T. kivui* shows strong potential for future large-scale CO_2-based fermentations.

Process simulations represent an essential tool for evaluating the technical and economic feasibility of emerging biotechnological pathways. In the field of gas fermentation, the literature to date has mainly focused on bioethanol production from syngas, with limited attention devoted to alternative products such as acetic acid. For example, Ardila et al., 2014 employed Aspen Plus® to simulate ethanol production from sugarcane bagasse gasification [14]. The fermentation step was modeled with a stoichiometric reactor, introducing syngas and a pure water medium, simplifying by omitting biomass required for microbial growth. Similarly, Rao et al., 2005 used both equilibrium and stoichiometric models for small-scale simulations [15]. Chen et al., developed a metabolic model for a bubble column reactor, highlighting the benefits of recycling unconverted gas to improve ethanol titer and gas utilization while emphasizing the importance of efficient gas-liquid mass transfer [16]. Michailos et al., 2017 modeled a CSTR at 311 K and 0.15 MPa, using bagasse-derived syngas to produce ethanol while recycling acetic acid and unreacted gases to enhance process efficiency [17]. Pardo-Planas et al., 2017 simulated a hybrid gasification–fermentation process for ethanol from switchgrass, using a stoichiometric reactor to represent the fermenter and including downstream distillation and drying units [18]. Despite their value, these studies remain limited to ethanol and do not explore the production of organic acids or other platform chemicals.

Most techno-economic assessment of gas fermentation similarly focus on bioethanol production [17,19–24]. Piccolo et al. compared enzymatic hydrolysis followed by fermentation (EHF) with gasification and subsequent syngas fermentation (GF), highlighting the greater maturity and industrial readiness of EHF, despite the need for further advancements to lower selling prices and enable large-scale deployment [25]. In contrast, GF remains less attractive due to high capital investment, energy-intensive product recovery, and moderate yields, resulting in elevated ethanol production costs. Swanson et al., 2010 simulated a hybrid gasification–fermentation pathway, reporting higher ethanol yields compared to conventional biochemical routes, but identified distillation as the major cost contributor [26]. Roy et al., 2015 emphasized the influence of feedstock type, heat recovery, and conversion technology selection on the economic and environmental performance of miscanthus-based ethanol production [24]. Michailos et al., 2017 conducted a feasibility study of ethanol production via bagasse gasification and fermentation, identifying low yields as a consequence of mass transfer limitations associated with poorly soluble CO and H_2 substrates [17]. De Medeiros et al., 2020 demonstrated that enhancing gas–liquid mass transfer in a bubble column reactor significantly improves efficiency and reduces costs [27]. Regis et al., 2023 performed a techno-economic analysis of ethanol production from switchgrass via gasification–fermentation, recommending nutrient cost reduction and reactor redesign to improve feasibility [20]. In a broader context, Choi et al., 2009 assessed the production of polyhydroxyalkanoates (PHA) through gasification–fermentation, showing cost advantages over sugar-based fermentation, with hydrogen co-production contributing positively to economic performance [28]. None of these processes are currently commercially viable, emphasizing the need for technological advances and reduced reactant costs, particularly for hydrogen as emphasized by Piccolo et al., 2009 and Regis et al., 2023 [19,20].

To the best of the authors' knowledge, no comprehensive simulation, techno-economic evaluation, or environmental assessment of acetic acid production via gas fermentation has been published to date. In particular, no study addresses the integration of CO_2 captured from biogas upgrading with H_2 from electrolysis for bio-acetic acid synthesis. Furthermore, no research has explored the downstream purification of highly diluted fermentation broths to produce glacial acetic acid, nor the influence of operating pressure on productivity and co-products formation. From an environmental standpoint, the lack of life cycle assessments on this process prevents a meaningful comparison with fossil-based acetic acid production routes. Only one study has assessed the environmental impacts, specifically global warming potential and primary energy demand, of comparing individual and integrated production routes for acetic acid, ethanol, and urea within a carbon capture and utilization system [29].

This study addresses these gaps by developing the first integrated process simulation of glacial bio-acetic acid (99.9 wt%) production from CO_2 and H_2, combining upstream gas purification, microbial fermentation, and downstream separation. Hydrogen is supplied through alkaline water electrolysis, the most mature and widely adopted technology for green hydrogen production; as discussed in Section S1 of the Supplementary Materials. The CO_2 used in the process is captured from the upgrading of biogas to biomethane via monoethanolamine (MEA)-based chemical absorption, with further details on CO_2 capture technologies provided in Section S2 of the Supplementary Materials. The fermentation step is modeled as a bubble column reactor, as discussed in Section S3 of the Supplementary Materials. Regis (2024) developed a 1D industrial-scale bubble column model for producing acetic acid from CO_2 and H_2 using *T. kivui* [30]. Two headspace pressures (2 and 10 bar) are investigated, revealing trade-offs between productivity, formic acid formation, and capital requirements. Specifically, higher pressure improves acetic acid titer and reduces the number of fermenters required, but increases CAPEX and complicates purification due to formic acid generation. Conversely, lower pressure minimizes by-product formation and reduces compression costs but requires a larger number of fermenters. For the downstream process, acetic acid is purified from its highly diluted solution in water using a hybrid method combining solvent extraction and azeotropic distillation. Although acetic acid and water do not form an azeotrope, the liquid-vapor diagram for this mixture exhibits a pinch point at low acetic acid concentrations. As a result, dehydration via evaporation or simple distillation columns is not feasible. This separation strategy was selected based on an extensive literature review (see Section S4 of the Supplementary Materials).

The entire process is simulated in Aspen Plus® to achieve high-purity acetic acid (99.9 %) at industrial-scale quantities. Operating and capital costs were estimated, with scalability analyzed for multiple parallel fermenters to evaluate production costs. Furthermore, the environmental impact of the entire process is evaluated through the Life Cycle Assessment (LCA) methodology accordingly with ISO 14040-44: 2006. The study demonstrates the feasibility of producing bio-acetic acid from captured CO_2 and green H_2, while quantifying the economic and environmental performance of this novel bioprocess in comparison with conventional fossil-based routes.

2. Methods

2.1. Overview of the entire process

The process is simulated using Aspen Plus® Version 10 (AspenTech, Inc.) to solve material and energy balances and size the equipment required for a techno-economic analysis. The complete process diagram, shown in Fig. 1, is designed to produce bio-acetic acid. Specifically, the fermentation step (S-500) is preceded by an upstream phase (S-100 to S-400) to obtain the reactants, hydrogen, and carbon dioxide, and followed by a downstream phase (S-600 to S-800) for purifying acetic acid from a highly diluted solution.

The process was modeled to achieve an annual production of 37 kton of glacial acetic acid, matching the capacity of the single bubble column reactor in the model developed by Regis, 2024 [30]. This reactor size is comparable to single bubble columns used in gas fermentation for ethanol production [31]. While this scale represents a conventional small-scale plant for acetic acid production, it can be expanded by employing multiple fermenters in parallel. This approach mirrors LanzaTech's strategy in Gent, Belgium, where parallel fermenters are already utilized for ethanol production [32].

2.2. Hydrogen production

The hydrogen production process is simulated in Aspen Plus® Version 10 using the ELECNRTL thermodynamic method. Alkaline electrolysis (AEL) was chosen for hydrogen production due to its maturity, lower cost, and compatibility with the pressure conditions of fermentation [33]. The alkaline electrolyzer uses a 30 wt% aqueous potassium hydroxide (KOH) solution as the electrolyte. This widely used electrolyte ensures efficient ion conduction and offers high conductivity while preventing stainless steel corrosion at this concentration [34]. The simulation follows the approach developed by Sánchez et al., 2020 [35], as detailed in Section 5 of the Supplementary Materials. The stoichiometry of the reaction is given by Eq. (1).

$$H_2O \rightarrow H_2 + \frac{1}{2} O_2 \quad (1)$$

Additional information about the components included in the simulation can be found in Section S5 of the Supplementary Materials. The PFD of hydrogen production section is shown in Fig. 2.

The simulation encompasses all equipment required for reactant conversion and product separation, as well as heat exchangers and pumps to facilitate fluid movement. The electrolyzer (R-101) is modeled as an RSTOIC reactor, with the pressure set to match fermentation conditions and the temperature aligned with typical operating values for alkaline electrolyzers. The fractional conversion is defined based on a

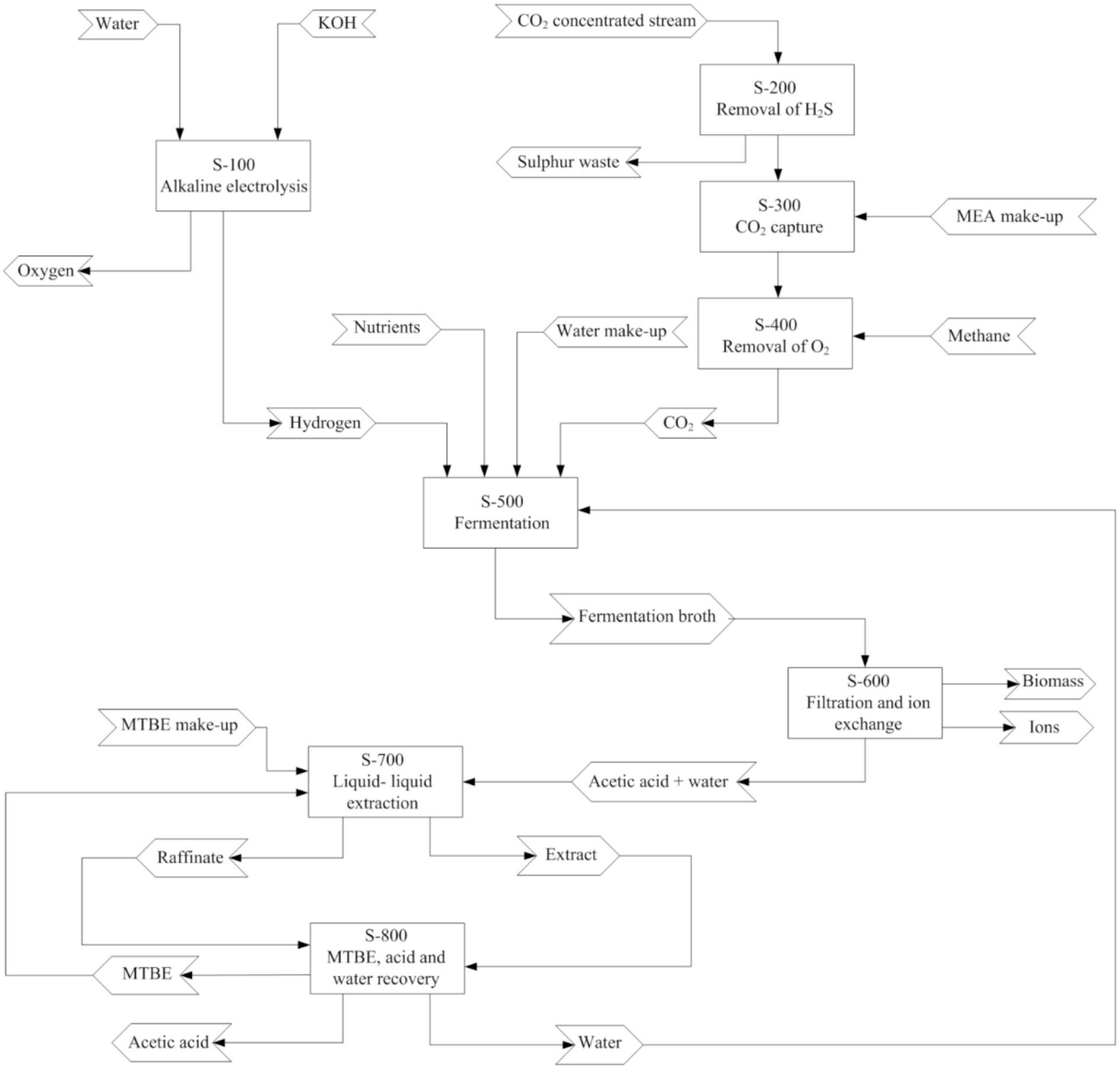


Fig. 1. Descriptive diagram of the production process of bio acetic acid.

water-to-hydrogen ratio of 1 L per Nm^3 of produced hydrogen, calculated using Eqs. (S5.3) and (S5.4) in Section S5 of the Supplementary Materials. The streams exiting the electrolyzer (streams 105 and 106) include unreacted liquid solution and produced gases, oxygen in stream 105 and hydrogen in stream 106. These streams are fed into flash separators (F-101 and F-102) to separate the gaseous streams (108 and 110) from the liquid ones (107 and 109). The separated liquid streams are first pressurized via pumps (P-102 and P-103) and then cooled to the feed temperature using a coaxial tube heat exchanger (E-102). Additionally, a second heat exchanger (E-101) dissipates the heat generated by the electrolyzer. The sizing of the electrolyzer is based on the model proposed by Sánchez et al., 2020, which defines the construction characteristics of a single stack using key assumptions [35]. These include an electrical power consumption of less than 0.5 MW, consistent with the state-of-the-art for alkaline electrolyzers, a current density of 0.4 A. cm^{-2}, and an active cell area of 1000 cm^2.

2.3. Carbon dioxide capture

The CO_2 capture process is simulated in Aspen Plus® Version 10 using the ENRTL-RK thermodynamic method. The chosen CO_2 capture method is chemical absorption with MEA, the most widely used technology for industrial-scale processes today. The incoming gas flowrate, detailed in Section S6 of the Supplementary Materials, is 6830.56 Nm^3. h^{-1}, consisting primarily of carbon dioxide (≈61 %) and nitrogen (≈31 %), with traces of methane, hydrogen, carbon monoxide, and hydrogen sulfide. Being CO_2 the product of interest, it must have the highest purity for the fermentation step. However, due to its acidic properties similar to CO_2, H_2S would also be absorbed in the amine solution. To address this issue, H_2S is removed in the S-200 purification section using the LO-CAT process, suited for low concentrations [36]. Details on the S-200 simulation are provided in Section S6.

After pre-treatment, the gas proceeds to the S-300 absorption section for CO_2 capture. The carbon dioxide absorption process uses two packed columns in series: one for CO_2 capture and the other for solvent regeneration. The solvent consists of 30 wt% MEA, offering the best balance between maximizing CO_2 absorption and minimizing corrosion and losses [37]. Additionally, 6.5 wt% CO_2 remains in the solvent, as complete removal during regeneration is assumed unfeasible. The remainder of the solvent is water. Details of the components used in the simulation and the chemical model for the absorption and stripping columns are provided in Section S6 of the Supplementary Materials.

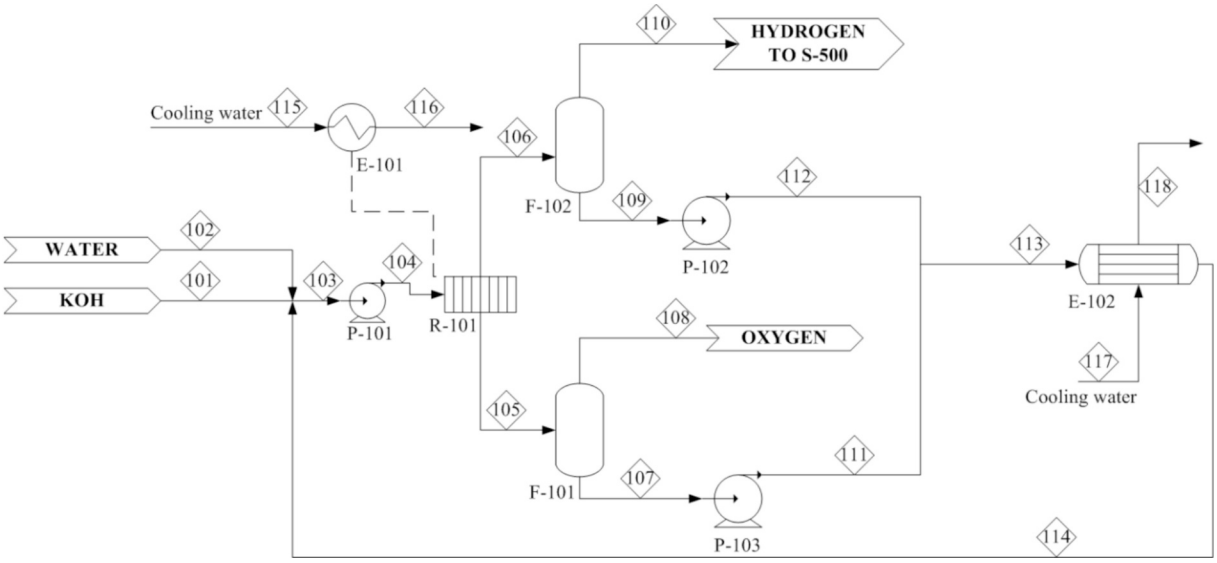


Fig. 2. PFD of section S-100 for the production of hydrogen.

The process targets are a CO_2 capture efficiency above 90 %, regeneration energy consumption below 5 $MJ.kg^{-1}$ captured CO_2 (state-of-the-art for MEA absorption [37]), CO_2 purity over 99 %, and an oxygen-free output stream.

Fig. 3 presents PFD of the CO_2 capture unit (S-300).

The absorber (C-301) operates at ambient pressure, while regeneration (C-301) is more effective at higher pressure. To achieve this, pump P-301 raises the pressure to 1.8 bar. For MEA-CO_2 mixtures, pressures above atmospheric levels improve stripping efficiency, but exceeding 2 bar risks MEA degradation [38]. Higher pressure increases the mixture's saturation temperature, raising overall temperatures. Following Madeddu et al., 2019, the inlet stream (stream 305) should be maintained 2 °C below the saturation temperature to optimize stripping efficiency [38]. A key challenge in the process is the high energy demand of the reboiler (E-303) in the stripping column. To mitigate this, the thermal energy of the regenerated solvent (stream 312) is used to preheat the solvent to be regenerated (stream 301) via a heat exchanger (E-301). This not only preheats the amine solution but also partially cools the solvent returning to the absorber. However, the solvent is not cooled enough, requiring an additional heat exchanger (E-304) to lower the temperature to the column inlet level. As the process is cyclical, water (stream 314) and amine (stream 315) must be replenished to compensate for inevitable losses. The procedures for column sizing are provided in Section S6 of the Supplementary Materials.

Excluding CO_2 and H_2S, removed in section S-200, the remaining gases in the feed stream exit the absorber in the gaseous stream (stream 303). The liquid stream leaving the absorber (stream 301) contains CO_2, water, and a small amount of oxygen (0.07 wt%), likely due to its solubility in CO_2. Since the final stream (stream 311) will be metabolized by anaerobic bacteria, oxygen must be removed. This is achieved in the second purification section (S-400) using a catalytic oxidation process with a platinum-based catalyst [39]. The PFD and details of S-400 are provided in Section S6 of the Supplementary Materials.

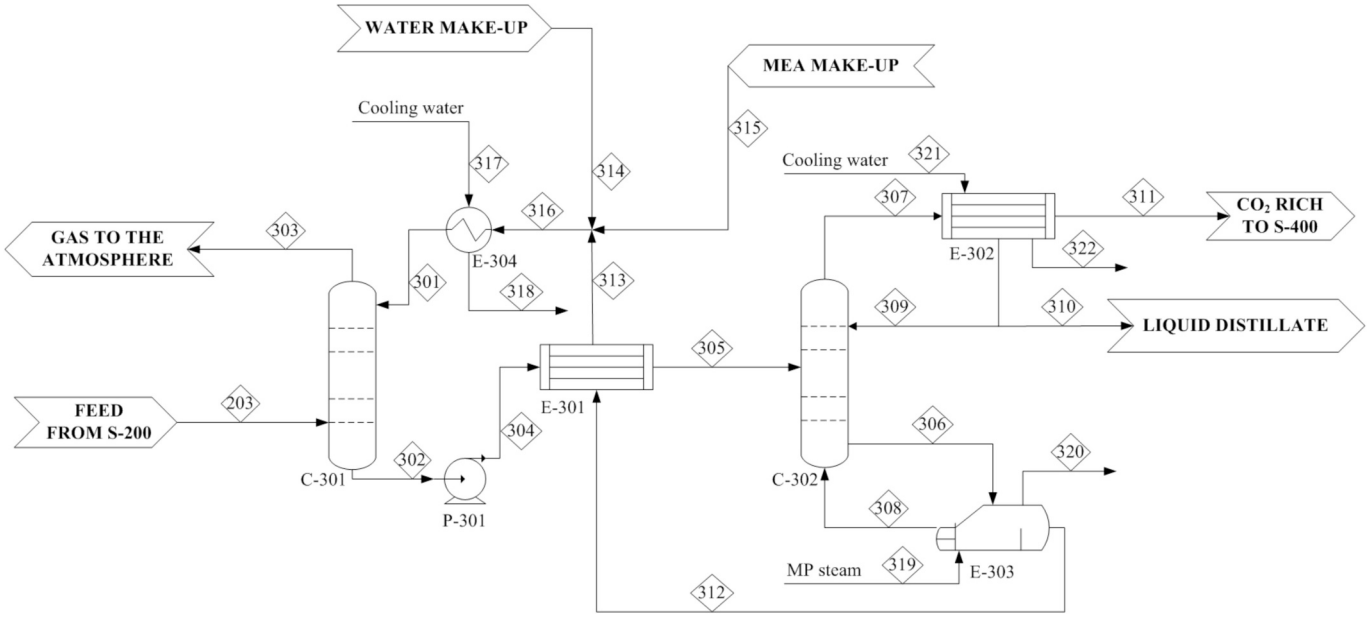


Fig. 3. PFD of section S-300 for CO_2 capture.

2.4. Fermentation

The fermentation process is simulated in Aspen Plus® Version 10 using the NRTL thermodynamic method. Details of the components used in the simulation are provided in Section S7 of the Supplementary Materials. The process was simulated at two fermenter headspace pressures, 2 bar and 10 bar, based on Regis, 2024 [30]. The study developed an industrial-scale bubble column fermenter model to identify optimal conditions for pressure, inlet flow rates, and gas composition to maximize acetic acid productivity under steady-state conditions. The optimal biomass concentration was found to be 5 $g.L^{-1}$. In the model a total reactor volume of 862 m3 was selected, consistent with capacities reported for industrial BCRs [40]. An outlet acetic acid concentration of 15 $g{\cdot}L^{-1}$ was imposed, corresponding to the inhibition threshold beyond which productivity declines [30]. Based on model outputs, the residence times required to reach this concentration at steady state were 2 h 28 min at 2 bar and 1 h 42 min at 10 bar. At 10 bar, acetic acid productivity and gas conversion rates are maximized, but formic acid complicates broth purification. At 2 bar, formic acid production is negligible, and compression costs are lower, but acetic acid productivity and gas conversion rates drop to 63 % and 65 %, respectively, compared to 10 bar. Regis, 2024 model allows for calculating gas conversion and determining the amounts of CO_2 and H_2 required to produce acetic acid, biomass, and formic acid. At 2 bar, producing 1 kg of acetic acid requires 1.71 kg of CO_2 and 0.14 kg of H_2, while at 10 bar, it requires 1.85 kg of CO_2 and 0.15 kg of H_2 [30]. These differences result from pressure-induced changes in dissolved substrate concentrations, which affect bacterial kinetics. The process flow diagrams for fermentations at 2 bar and 10 bar are shown in Figs. 4 and 5, respectively.

The bubble column fermenter (R-501) is modeled as an RSTOIC reactor operating at 66 °C, with a headspace pressure of 2 bar or 10 bar depending on the simulation. Acetic acid production follows the reaction in Eq. (2).

$$2CO_2 + 4H_2 \rightarrow CH_3COOH + 2H_2O \quad (2)$$

At a headspace pressure of 2 bar, only the previous reaction is considered, as formic acid production is negligible compared to acetic acid. However, at 10 bar, the formic acid production reaction Eq. (3) must also be included.

$$CO_2 + H_2 \rightarrow HCOOH \quad (3)$$

For simplification, *T. kivui* and its medium are excluded from the simulation. However, although the water entering the reactor depletes the nutrients required for bacterial growth, the latter are accounted in the economic analysis. Unconverted gas is recirculated to the reactor after recompression. Gases entering the reactor are pressurized 10 % above the column bottom pressure to offset sparger pressure drops and heated to 66 °C via heat exchanger E-502. For a 2-bar headspace pressure, H_2 and CO_2 streams are already at the required pressure. At 10 bar, additional compression is needed using compressors C-502 and C-503, with heat exchanger E-503 required to raise CO_2 stream water vapor above the dew point. Water recirculated from the acetic acid purification section (stream 823) and make-up water (stream 501) are pressurized to the column bottom pressure using pump P-501.

2.5. Acetic acid purification

Efficiently purifying acetic acid from a fermentative broth requires two essential preliminary steps: filtration and ion exchange. Filtration removes solid components, such as residual cellular material, while ion exchange eliminates salts and other ions. Details on these processes are provided in Section S8 of the Supplementary Materials. Acetic acid is purified from water using the HEDP process (hybrid extraction/distillation), which combines liquid-liquid extraction and azeotropic distillation. Chilev et al., 2021 highlight its efficiency over conventional methods due to reduced product and solvent loss, fewer stages needed in the distillation column, and lower energy consumption [41]. In this process, an organic solvent extracts acetic acid from water. Methyl tert-butyl ether (MTBE) was chosen for its high extraction capacity and ability to form an azeotrope with water at low temperature (51.6 °C) and concentration (4 wt%), minimizing energy use during azeotropic distillation. The distillation step recovers acetic acid at 99.9 % purity (suitable for the GAA market) from the bottom, while water and MTBE, forming the distillate, are separated via a decanter. MTBE is recirculated for reuse, and purified water is returned to the fermentation section (S-500). The purification section was simulated using Aspen Plus® V10, employing the NRTL-HOC thermodynamic method, recognized as the most suitable for dealing with organic acids [41]. In the entire process no pressure losses were considered. Details of the components used in the simulation are provided in Section S8 of the Supplementary Materials. Fig. 6 shows the process diagram of the extraction section.

The feed stream (508) from the fermentation section (S-500), when conducted with a headspace pressure of 2 bar, contains 1.5 wt% acetic acid and 98.5 wt% water, assuming complete removal of salts and soluble components via ion exchange resins. The flowrate to be processed is 284,923 $kg.h^{-1}$. The extraction column (C-701), modeled using the EXTRACT module, was designed to recover 100 % of the acetic acid in the feed into the organic extract. Details of the column modelling are provided in Section S8 of the Supplementary Materials.

The PFD of acetic acid, water and solvent recovery section (S-800) of the hybrid process is represented in Fig. 7.

The azeotropic distillation column (C-801) was modeled using the

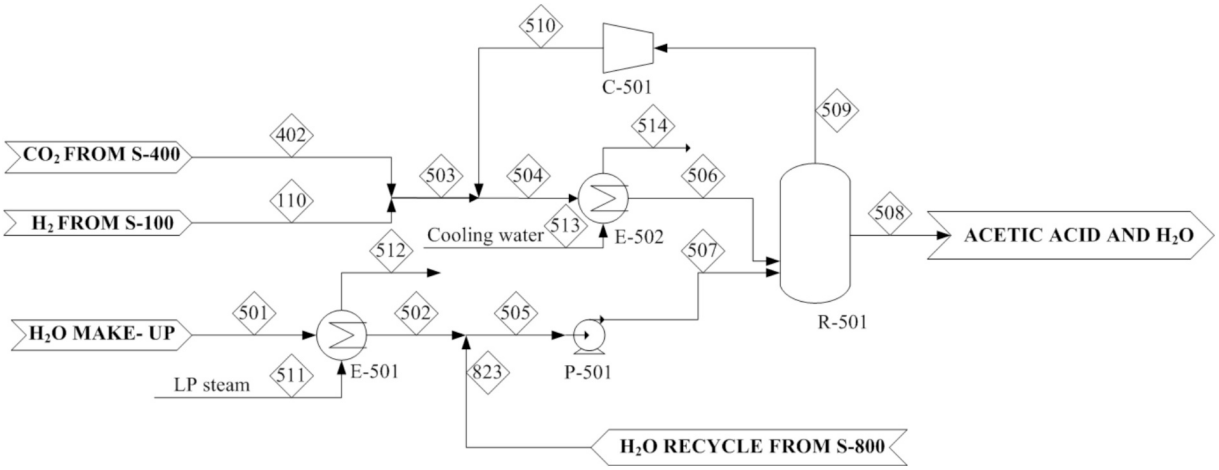


Fig. 4. PFD S-500 for fermentation section with 2 bar headspace pressure in the fermenter.

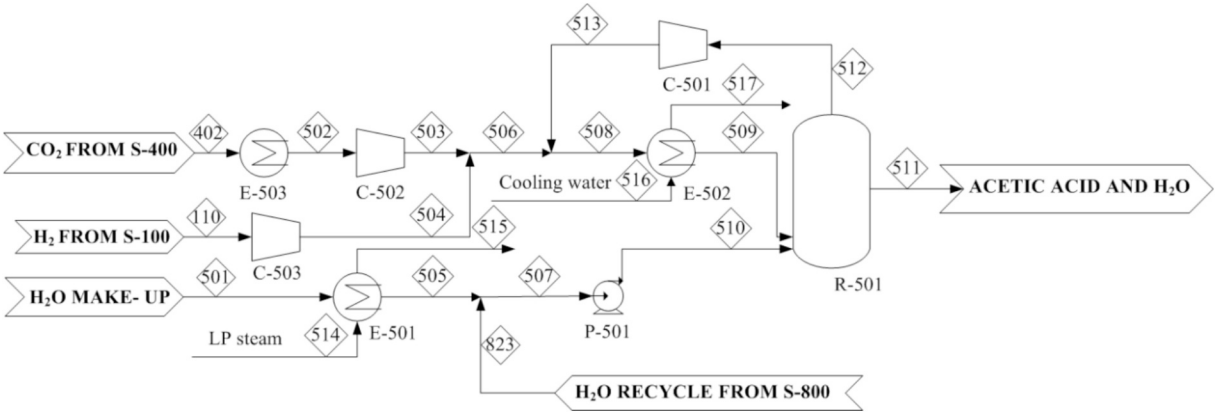


Fig. 5. PFD S-500 for fermentation section with 10 bar headspace pressure in the fermenter.

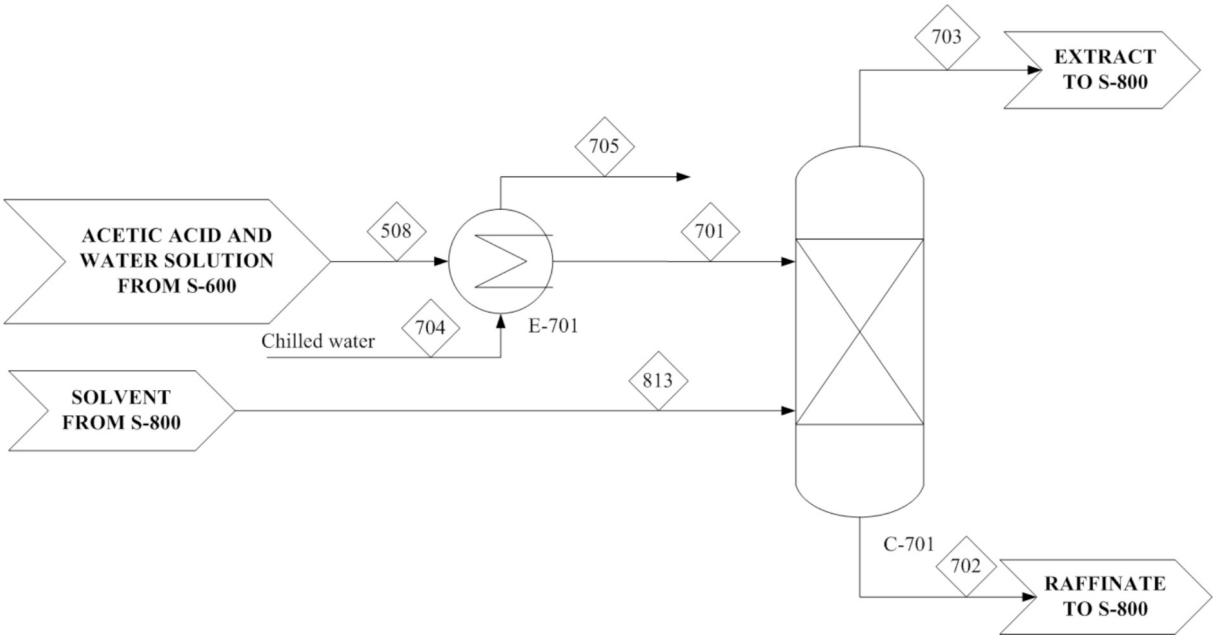


Fig. 6. PFD S-700 for the extraction section.

RADFRAC module to achieve 99.9 % acetic acid purity at the bottom (stream 806, GAA target). This stream is cooled to 30 °C in heat exchanger E-803 for transport and sale. At the column head (stream 807), a mixture of MTBE and water is directed to a decanter (D-801) for separation. Before decantation, the MTBE-water stream is combined with the overhead product (stream 824) from the distillation column (C-802), which treats the aqueous raffinate from the extraction section. MTBE losses are compensated with a make-up stream (809). The decanter operates at 20 °C, maintained using heat exchanger E-804, and the recovered MTBE is recirculated to the extraction column (C-701). The separated water (stream 812) is combined with raffinate (stream 702) and purified in distillation column C-802, also modeled with RADFRAC, to obtain 99.99 % pure water. The feed to C-802 is preheated to 50 °C in exchanger E-805, as entering at 20 °C disrupts column operation. From the column bottom (stream 822), high-purity water is recovered, cooled to 66 °C in exchanger E-808, and recycled to the fermentation section (S-500). To maintain water mass balance and avoid recirculation issues, a purge stream (814) is included upstream of C-802. Sizing details for both distillation columns are provided in Section S8 of the Supplementary Materials.

2.6. Thermal integration

To enhance energy efficiency, Pinch Analysis was conducted using Aspen Energy Analyzer to optimize heat recovery systems and minimize utility consumption. This method maximizes heat exchange between process streams, achieving potential energy recovery, though it may increase fixed costs for heat exchangers. The software generates hot and cold composite curves, which illustrate the temperature-enthalpy relationship for heat removal and heat addition, respectively. These curves help identify the pinch point, where the temperature difference between streams is minimal. Utility usage is minimized by avoiding heat transfer between streams with a temperature difference at or below the pinch temperature, using cold utilities to cool streams above the pinch, or employing hot utilities to heat streams below the pinch. Throughout the process, a minimum temperature difference between the hot and cold sides (ΔT_{min}) of 10 °C was maintained.

2.7. Economic analysis and KPIs

2.7.1. Total project investment evaluation

The first step in the economic analysis is evaluating the Total Project

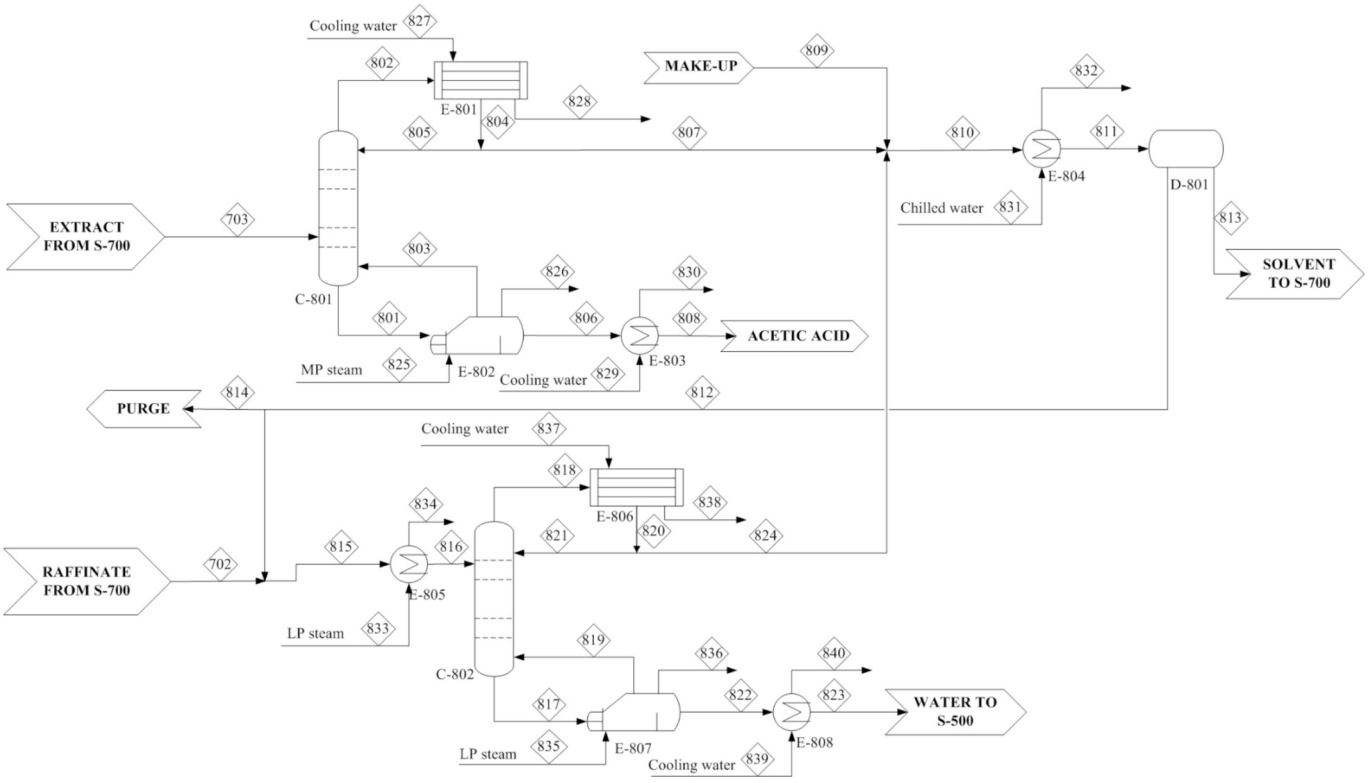


Fig. 7. PFD S-800 for acetic acid, water and solvent recovery section.

Investment (TPI) by determining the Purchase Equipment Costs (PEC) for each process component. Using Aspen Process Economic Analyzer (APEA) in Aspen Plus® V10, equipment is sized, and costs are estimated based on a database from Engineering, Procurement, and Construction (EPC) companies. For some plant sections, a different method was used to assess the PEC. Costs were obtained from literature or manufacturer quotes and scaled to the required size using the relationship in Eq. (4) when pricing was available for a different size or capacity.

$$\frac{PEC_a}{PEC_b} = \left(\frac{A_a}{A_b}\right)^{\gamma} \tag{4}$$

In Eq. (4), A represents the equipment cost attribute (size or capacity), and γ is a cost exponent factor, set to 0.6 following the six-tenths rule [42]. For the hydrogen production section (S-100), the PEC of the electrolyzer was calculated using the reference value of 510 €.kW^{-1} (2023) [43]. For the LO-CAT process, the PEC of the H_2S removal reactor (R-201) was scaled using data from the supplementary materials in Bressanin et al., 2020 [44]. In the O_2 removal section, the PEC of the catalytic reactor (R-401) was scaled based on Peppel et al., 2017 [39]. The catalyst, composed of 99 % γ-alumina and 1 % platinum, was costed using literature data [45,46].

All PECs were scaled to 2023, the chosen base year, using Eq. (5).

$$\frac{PEC_1}{PEC_2} = \frac{CEPCI_1}{CEPCI_2} \tag{5}$$

In Eq. (5), CEPCI represents the Chemical Engineering Plant Cost Index, with subscripts 1 and 2 indicating the year of the available cost and the base year, respectively [42]. The Installed Equipment Cost (IEC) for each piece of equipment is derived from the PEC using Eq. (6).

$$IEC = \frac{PEC}{1 - \alpha_1 - \alpha_2} \tag{6}$$

In Eq. (6), α_1 and α_2 are coefficients accounting for installation costs, materials, and labor, with values of 0.24 and 0.08, respectively [45]. The Total Equipment Cost (TEC) was calculated as the sum of all IECs, with additional costs for the warehouse (1.5 % of TEC) and site development (9 % of TEC) added to determine the Total Installed Cost (TIC). The Total Capital Investment (TCI) was then obtained by adding indirect expenses to the TIC, including site expenses (20 % of TCI), offices and construction taxes (25 % of TCI), and contractual contingencies (3 % of TCI). Finally, the Total Project Investment (TPI) was determined by adding generic expenses, such as permits and start-up costs, estimated at 10 % of TIC [42].

2.7.2. Operational cost evaluation

To evaluate total operating costs, variable and fixed operating costs were analyzed. Variable costs, considered only during plant operation, include raw materials, utilities, and waste handling. For hydrogen production, raw material prices included water (0.021 €.m^{-3} from APEA) and KOH (465 €.ton^{-1} [47]). CO_2 capture considered MEA (1.1 €.kg^{-1} [48]) and chemicals for H_2S removal, along with methane (0.13 €.Nm^{-3} [49]) for O_2 removal in section S-400. In the fermentation section, costs included water, nutrients for bacterial growth, and the bacterium inoculum from a microbial bank. For the downstream phase, the cost of MTBE (653 €.t^{-1} [49]) was included. In section S-600, reactant costs for resin regeneration were 630 €.ton^{-1} for HCl (37 % solution) and 130 €.ton^{-1} for NaOH. Annual replacement was assumed for MEA, MTBE, and KOH to account for potential degradation or contamination.

In 2023, Italy's total energy supply relied on fossil fuels for 79 % of its needs, while electricity generation was 54.1 % fossil-based [50]. In this context, the economic analysis considers an electricity price of 0.07 €.kWh^{-1}. An additional scenario was also evaluated using a price of 0.13 €.kWh^{-1}, which reflects the average electricity cost in Italy in 2023, while 0.07 €.kWh^{-1} corresponds to the European average [51]. Italy is on track to meet the emissions reduction and energy efficiency targets set in its National Energy and Climate Plan (NECP) for 2030. By that year, 63.4 % of gross electricity consumption is expected to be covered by renewable sources, and 39.4 % of total final energy consumption is projected to come from renewables [52]. For 2030, the base scenario adopts an electricity price of 0.07 €.kWh^{-1}, with an additional scenario

assessed 0.11 €.kWh^{-1} [53]. Despite significant progress in integrating renewable energy into the national grid, Italy is expected to remain substantially reliant on fossil fuels, particularly natural gas, through 2030. This dependency raises concerns about energy security and increases exposure to market volatility and price fluctuations. Concurrently, the growing share of variable renewable energy introduces new challenges for balancing electricity supply and demand, requiring extensive investment in grid infrastructure, energy storage, and flexible market mechanisms. By 2030, electricity prices are projected to decline during midday hours due to abundant solar generation. However, price volatility is expected to intensify, especially during winter peak demand periods when renewable output is limited. In these conditions, dispatchable generation will be essential to ensure system stability. Consequently, sharp price spikes are anticipated during low-renewable periods, highlighting the enduring need for conventional power sources to support grid reliability.

Thermal utilities necessary for the required operations were implemented, and their costs, along with electrical expenses, were analyzed using APEA. Variable costs also included wastewater and waste chemical treatments. Wastewater treatment addresses the purged aqueous stream from the recovery section (S-800), containing MTBE traces and water-soluble components not removed during preliminary purification. This treatment costs 3 €.m^{-3} [42]. Waste chemical treatment involves replacing solvents, KOH (S-100), MEA (S-300), and MTBE (S-700), at an estimated cost of 200 €.ton^{-1} [42].

Fixed operating costs, including labor and overheads, were fully charged regardless of plant capacity utilization. Operating labour calculations are detailed in Section S9 of the Supplementary Materials. Fixed operating costs include salaries along with expenses for general overhead, maintenance, insurance, and taxes. Overhead costs, covering research and development, support equipment, and patented technology use, are estimated at 60 % of salaries. Maintenance costs are 2 % of the Total Equipment Cost, while taxes and insurance are calculated at 1.5 % of the Total Installed Cost.

2.7.3. Discounted cash flow analysis

After estimating the total investment and operational costs, a discounted cash flow rate of return analysis determines the minimum selling price for fermentation-derived acetic acid, ensuring full recovery of investments and expenses. This analysis adjusts the product's final price iteratively until the net present value (NPV) of the process equals zero. NPV is calculated by subtracting the Total Project Investment (TPI) from the cumulative cash flows over the plant's lifespan, as shown in Eq. (7) [54].

$$\mathrm{NPV} = \sum_{t=1}^{PL} \frac{\mathrm{TAS} - \mathrm{TPC} - \mathrm{IT}}{(1+\mathrm{DR})^t} - \mathrm{TPI} \tag{7}$$

In Eq. (7), the total cash flow is calculated as the Total Annual Sales (TAS), representing annual revenue with a positive sign, minus the Total Production Costs (TPC) and Income Taxes (IT). The denominator incorporates an interest factor that varies annually, determined by the discount rate (DR). The index '*t*' represents the plant's operating year, ranging from 1 to the Plant Life (PL), assumed to be 20 years for this process, aligning with typical chemical plant lifespans. The parameters for the discounted cash flow analysis were based on Short et al., 1995 [55]. The plant is assumed to be in Europe, where the tax rate is 33 % [56]. A 6-month startup period was considered, during which revenues are 50 % of nominal values, fixed operating expenses remain at 100 %, and variable operating expenses are at 75 %. Total project investment is allocated over the three years before startup: 8 % of TPI in year −3, 60 % in year −2, and 32 % in year −1. Additionally, working capital equal to 5 % of TPI is included in the final year. Depreciation is calculated at 200 % using the declining balance method over a 7-year recovery period. During this time, product sales revenues are less than depreciation expenses, resulting in no taxes being applied. Local taxes are excluded due to the unspecified plant location within Europe. Table 1 provides a summary of the parameters used in the discounted cash flow analysis.

2.7.4. Key performance indicators

To evaluate the profitability and efficiency of the process, Key Performance Indicators (KPIs) measuring energy performance and process efficiency were analyzed. These KPIs provide a basis for comparing technologies and identifying areas for improvement. For alkaline electrolysis, the selected KPI is the specific energy consumption per kilogram of hydrogen produced. Industrial-scale alkaline electrolyzers typically consume 55–60 kWh per kilogram of hydrogen [57]. In the CO_2 absorption process, three KPIs were considered: specific energy consumption, CO_2 capture efficiency, and stream purity. Specific energy consumption is the energy used in the reboiler of the stripping column per unit of CO_2 captured, typically ranging from 3.5 to 5 MJ.kg^{-1} [37]. The target CO_2 recovery rate is 90 %, with a purity goal of 99 % for the outgoing stream. For the downstream section, the chosen KPIs include acetic acid stream purity, acetic acid recovery, solvent consumption, and specific energy consumption for heating and cooling. Acetic acid recovery is calculated as the ratio of the acetic acid flowrate in the product stream to that in the feed exiting the fermentation section (S-500). Solvent consumption is defined as the ratio of MTBE make-up flowrate to the product flowrate. For the overall process, carbon efficiency was selected as a KPI. It is defined as the ratio of carbon flow in the acetic acid product (stream 808) to the carbon flow in the CO_2 feed entering the capture section (stream 203). The formulas for KPI calculations are detailed in Section S9 of the Supplementary Materials.

2.8. Environmental assessment

Life cycle assessment (LCA) was performed with SimaPro 9.5 software and database Ecoinvent 3.11 accordingly with ISO 14040-14,044:2006. LCA includes four phases (goal and scope definition, inventory, impact assessment and interpretation) following reported.

The goal of the study was the evaluation of the environmental impacts of the production of glacial bio-acetic acid through the process depicted in Fig. 1 and described in paragraphs 2.1–2.5. The scope of the study was to understand if the bio-acetic acid production could be environmentally sustainable at industrial scale compared with the current chemical production of glacial acetic acid and if it could represent an environmentally effective CCSU technology. Additionally, a carbon pricing sensitivity analysis (0–200 €.tonCO_2^{-1}) was conducted to assess how carbon taxes, based on LCA-derived environmental impacts, would influence the economic competitiveness of the bio-based process relative to the conventional fossil-based route.

The functional unit (FU) was 37 kton.y^{-1} of glacial acetic acid, since it was the amount produced for which the plant system was modeled on Aspen Plus® (Version 10). This type of FU agreed with that one of Miranda et al., 2023 [29], that is the only available study about

Table 1
Discounted cash flow analysis parameters.

Plant life	20 years
Discount rate	10 %
General plant depreciation	200 % declining balance
General plant recovery period	7 years
Federal tax rate	33 %
Financing	100 % equity
Construction period	2.5 years
First 6 months' expenditures	8 %
Next 12 months' expenditures	60 %
Last 12 months' expenditures	32 %
Working capital	5 % of TPI
Start-up time	0.5 years
Revenues during start-up	50 % of normal
Variable cost during start-up	75 % of normal
Fixed cost during start-up	100 % of normal

environmental impact performed on acetic acid produced as a carbon capture and use system.

The process analyzed in the present work includes an upstream phase to purify reactants, a fermentation stage, and a downstream step to concentrate the dilute culture broth into glacial acetic acid. H_2 is generated via alkaline water electrolysis, while CO_2 is captured using monoethanolamine absorption. The CO_2 originates from upgrading biogas into bio-methane, derived from anaerobic digestion of the organic fraction of the municipal solid waste. Fermentation was modeled at 2 headspace pressure. The purification of acetic acid occurs with a hybrid process, which combines liquid-liquid extraction and azeotropic distillation using methyl tert-butyl ether as solvent, achieving 99.9 wt% purity. In this assessment, the required energy, the consumed reagents, and the produced emissions were referred to the FU. The boundary conditions were depicted in Fig. 1, and they included from cradle (extraction of raw material) to gate (glacial acetic acid production) approach [58].

Following Thushari et al., 2020 only the direct consequences of glacial bio-acetic acid production were considered, and the environmental impacts of the infrastructures were not included, because they were less important to the overall impact results of the plant investigated [58].

The glacial bio-acid production system included a foreground and background system [59]. The foreground system is directly involved with the reference flow and the background system is linked with the foreground system, including energy production and chemical supply [58].

The Life Cycle Inventory (LCI), detailing all inputs and outputs involved in glacial acetic acid production, is presented in Tables S10.1, S10.2, and S10.3 within Section S10 of the Supplementary Materials. The primary data came from paragraphs 2.1–2.5. The secondary data were taken from the database Ecoinvent 3.11. The study was geo-contextualised in Italy and the Italian energy mix was considered. The Attributional LCA with mass allocation of multi-outputs was applied. Attributional LCA means a modelling approach by which inputs and outputs are attributed to the FU of a product system linking the unit processes of the system according to a normative rule. Life Cycle Impact assessment (LCIA) was performed with the ReCiPe Midpoint (H) 2016 to obtain a general overview of the impact of the studied process on the different impact categories. The interpretation analysis consists of evaluating the obtained impacts according to the involved flows. To prove the consistency a decrease of 5 % in the glacial bio-acetic production was assumed according to the uncertainty parameters reported in Clavreul et al. 2012 [60]. During the interpretation phase, for the identified process hotspots a possible mitigation action will be proposed.

3. Results and discussion

3.1. Results of the simulations

The alkaline electrolysis plant for H_2 production, described in Section 2.2, operates continuously with recirculated water. Stream 110 contains 80.17 wt% hydrogen and 19.83 wt% water. As the hydrogen is used with water in the fermentation section (S-500), high purity is not required. A single stack produces 166.39 ton.y^{-1} of hydrogen with a specific energy consumption of 56.68 kWh.kg^{-1}, within the typical range of 48.96–58.98 kWh.kg^{-1} [61]. Details on hydrogen flow and stack sizing are provided in Section S11 of the Supplementary Materials.

The carbon dioxide capture process using MEA, detailed in Section 2.3, operates continuously with recirculated solvent. To compensate for losses, 0.10 kg.h^{-1} of fresh amine and 1073 kg.h^{-1} of water are added. The process recovers 91.90 wt% of CO_2 from the incoming stream, achieving 99.50 wt% CO_2 purity in the final stream (stream 402). The specific energy consumption is 4.98 MJ.kg^{-1}, consistent with literature [37]. Stream 402, used as a reactant in the fermentation section (S-500), is oxygen-free. Key specifications of the CO_2 stream, along with the sizing and details of the absorption and stripping columns in the CO_2 capture section, are provided in Section S11 of the Supplementary Materials.

The fermentation section for acetic acid production, described in Section 2.4, operates continuously recycling unconverted CO_2 and H_2 to minimize waste and emissions. At 2 bar headspace pressure in the bubble column, 37 kton.y^{-1} of acetic acid are produced, increasing to 53.94 kton.y^{-1} at 10 bar, along with 0.17 kton.y^{-1} of formic acid [30]. Purified water from section S-800 supplies part of the required water. Details on raw materials and conversions are provided in Section S11 of the Supplementary Materials.

The purification process of acetic acid from fermentation broth is described in Section 2.5. This continuous process recirculates MTBE as the solvent and uses purified water as a reactant in the fermentation section (S-500). To compensate for unavoidable losses, a solvent make-up of 305 kg.h^{-1} is required. A purge is also implemented to prevent inert buildup in the system, though it contributes to MTBE losses. Acetic acid recovery in stream 808 achieves 99.80 wt% with 99.90 wt% purity, meeting GAA sale requirements. Solvent consumption is 71.56 g.kg^{-1}, and utilities energy consumption is 124.57 MJ.kg^{-1}. The water stream exiting from the purification section (stream 823) has 99.99 wt% water purity and a 97.50 wt% recovery compared to inlet stream 508. Sizing results for the HEDP extraction (S-700) and recovery section (S-800) equipment are detailed in Section S11 of the Supplementary Materials.

As detailed in Section 2.6, an energy analysis using the Pinch Analysis Method in Aspen Energy Analyzer aimed to reduce energy consumption by optimizing heat recovery systems. Energy integration was performed on the exchangers in the fermentation and purification sections, which had multiple heat flows to utilize. While the optimized design involved higher capital costs than the original heat exchanger design, significantly reduced operating costs offset these investments, leading to lower total costs over time. For the fermentation process at 2 bar headspace pressure, hot utility demand is entirely eliminated, and cold utility demand is reduced by 82 %, with a 20 % increase in capital costs. At 10 bar headspace pressure, hot utility demand is also eliminated, and cold utility demand decreases by 28 %, with a 5 % rise in capital costs. In the downstream section, the optimized design eliminates hot utility demand and cuts cold utility demand by 93 %, with a 21 % increase in capital costs compared to the initial heat exchanger design. The original and optimized heat exchanger designs for each section, are detailed in Section S11 of the Supplementary Materials. Integrating the entire process was unfeasible due to nearly vertical composite curve lines, indicating minimal enthalpy variation with temperature changes. This revealed insufficient heat for effective energy exchange between plant sections.

3.2. Results of the economic analysis

The hydrogen production process is outlined in Section 2.2, and the simulation results are detailed in Section 3.1. Electrolyser costs dominate capital expenditure, accounting for over 78 % due to their complexity, use of expensive corrosion-resistant materials, and advanced separation systems. Details on Total Project Investment and the percentage distribution of Purchase Equipment Costs are provided in Section S12 of the Supplementary Materials. Utilities make up the largest share of OPEX, with electricity as the main contributor, essential for splitting water into hydrogen and oxygen, though some energy is lost as heat by the electrolyser. Section S12 of the Supplementary Materials also outlines operating costs and the breakdown of variable operating costs per kilogram of hydrogen. The total investment for a plant producing 5.68 kton.y^{-1} of hydrogen is 39.81 M€, with fixed operating costs of 2.50 M€.y^{-1} and variable costs of 12.28 M€.y^{-1}. Applying the iterative method outlined in Section 2.7.3, the minimum hydrogen selling price required to achieve zero NPV was determined to be 3.77 €.kg^{-1} at an electricity cost of 0.07 €.kWh^{-1}. When the electricity price increased to 0.13 €.kWh^{-1}, the corresponding minimum hydrogen selling price

rose to 5.19 €.kg^{-1}.

The simulation was repeated for an additional scenario considering hydrogen production in 2030. The European Union's Strategic and Innovation Agenda 2021–2027 outlines 2030 targets for advancing electrolyser technology, focusing on greater efficiency, reduced management costs, and lower use of raw materials, particularly critical ones. Table 2 compares these targets with the 2021 state-of-the-art in alkaline electrolysis technology [43].

Higher current density reduces the number of cells required in the stack to achieve the same hourly productivity, contributing to a decrease in CAPEX alongside the drop in capital cost to 400 €.kW^{-1}. Electricity demand is also reduced, lowering OPEX. Additionally, less heat is generated by the electrolyser, reducing the cold utility demand for exchanger E-101 and its capital cost. For a hydrogen productivity of 5.68 kton.y^{-1}, the specific PEC for the electrolyser decreases from 2.13 €.kg^{-1}.y to 1.81 €.kg^{-1}.y. At an electricity price of 0.07 €.kWh^{-1}, electricity-related production costs drop from 1.91 €.kg^{-1} to 1.58 €.kg^{-1}, and cold utility costs decrease from 0.15 €.kg^{-1} to 0.12 €.kg^{-1}. As a result, the minimum selling price falls from 3.77 €.kg^{-1} to 3.17 €.kg^{-1}. When the electricity price increased to 0.11 €.kWh^{-1}, the corresponding minimum hydrogen selling price rose to 3.94 €.kg^{-1}.

The performance improvements assumed for alkaline electrolysis technology in the 2030 scenario are supported by well-defined technological development pathways outlined by the Clean Hydrogen Joint Undertaking and other European strategic initiatives. The reduction in specific electricity consumption is primarily due to the development of advanced electrode and membrane materials, improved cell designs, and optimization of key operating conditions such as temperature, pressure, and reactant flow [62]. The expected decrease in capital expenditure is enabled by modular mass production of electrolyzers, integrated system designs, and the replacement of critical raw materials with more abundant and lower-cost alternatives [63]. Operational costs are projected to decline as a result of increased component durability, lower electrochemical degradation rates, and the adoption of automated control and predictive maintenance systems [64]. Additional improvements such as shorter start-up times and greater operational flexibility are also anticipated, facilitating dynamic operation and better integration with variable renewable energy sources.

Beyond technological progress, the 2030 scenario is influenced by shifts in economic conditions, policy frameworks, and energy system configurations. Cost reductions are expected from economies of scale and growing market competition in both electrolyzer manufacturing and renewable electricity supply [65]. Policy developments, such as stricter carbon pricing, hydrogen quotas, and targeted funding mechanisms (e.g., EU Innovation Fund, Hydrogen Bank), are designed to reduce investment risks and accelerate deployment [66]. Meanwhile, the increasing share of variable renewable energy is reshaping electricity markets, enabling lower-cost electricity during surplus periods and supporting flexible hydrogen production [67].

Since literature prices typically reference smaller plant sizes than the 5.68 kton.y^{-1} target, the AEL *sec*tion was scaled up from a single-stack productivity of 166.39 ton.y^{-1} to match literature ranges. CAPEX was scaled using Eq. (4), and OPEX proportionally to productivity (with the electricity price assumed to be 0.07 €.kWh^{-1}). Fig. 8 presents the scaling-up results alongside literature data from Table S11.4 in Section S12 of the Supplementary Materials [68–76].

Table 2
Comparison of 2030 European targets and 2021 baseline values for the development of alkaline electrolysers.

Key performance indicator	State of the art (2021)	Target (2030)
Electric consumption (kWh.kg^{-1})	50	48
Capital cost (€.kW^{-1})	600	400
Operating costs O&M (€.(kg.d^{-1})$^{-1}$.y^{-1})	50	35
Start-up time (sec)	3600	300
Degradation (%.1000 h^{-1})	0.12	0.1
Current density (A.cm^{-2})	0.6	1
Use of critical raw materials (mg.W^{-1})	0.6	0

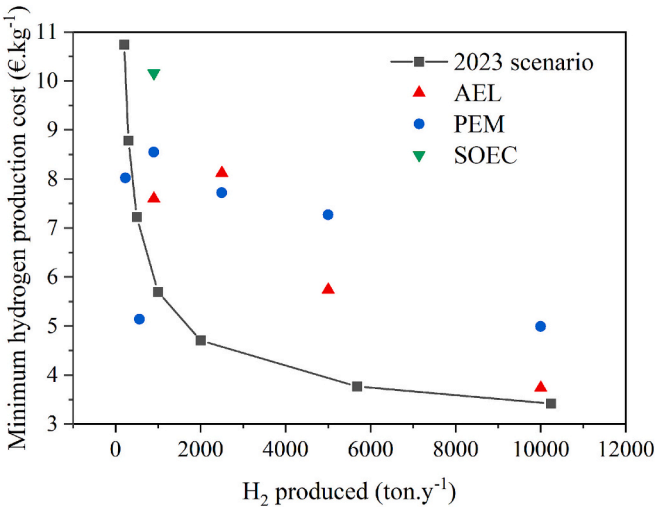


Fig. 8. Effect of plant scale on the minimum selling price of hydrogen (black squares). Also depicted are the selling costs from the literature of hydrogen produced through various electrolysis technologies (Red triangles: AEL; Blue dots: PEM; Green triangles: SOEC) at different scales.

The results show that the calculated hydrogen selling price is generally lower than most literature values. However, the produced hydrogen has a purity of 80.17 wt% as dehydration is unnecessary for subsequent fermentation.

The carbon dioxide capture process is described in Section 2.3, while the results of the simulation are reported in Section 3.1. The higher costs are primarily associated with the CO_2 capture section (S-300), with the absorber (C-301) and stripper (C-302) contributing 17 % and 27 % of the TEC, respectively. While the H_2S removal section also has a notable cost impact, the oxygen abatement section (S-400) incurs lower capital costs despite using a platinum-based catalyst, owing to the minimal O_2 to be removed. Details on Total Project Investment and the percentage distribution of Purchase Equipment Costs are provided in Section S12 of the Supplementary Materials. Utilities account for 76.52 % of operational expenses, driven largely by the energy-intensive solvent regeneration process. This process demands substantial medium-pressure steam (MPS) as the primary hot utility, contributing about 88.18 % of total variable costs. Section S12 of the Supplementary Materials also outlines operating costs and the breakdown of variable operating costs per kilogram of carbon dioxide. The total investment for a plant capturing 64.02 kton.y^{-1} of CO_2 is 2.12 M€, with annual fixed operating costs of 0.74 M€.y^{-1} and variable costs of 2.90 M€.y^{-1}. A minimum CO_2 selling price of 0.063 €.kg^{-1} ensures an NPV of zero, as determined through the iterative procedure in Section 2.7.3. The electricity price is assumed to be 0.07 €.kWh^{-1}; however, an increase to 0.11–0.13 €.kWh^{-1} results in cost variations of less than 1 % per kilogram of CO_2 captured.

Carbon capture plants are typically located downstream of cement factories, metallurgical plants, or power plants, with no economic analyses found for waste streams from biodigesters in the literature. Additionally, these plants generally operate at much larger scales than biodigesters. To bridge this gap, the carbon capture section was scaled up to align with literature sizes. CAPEX was estimated using Eq. (4), while OPEX was scaled proportionally to productivity. Fig. 9 compares these scaling-up results with literature data from Table S11.8 in Section S12 of the Supplementary Materials [77–86].

The results indicate that the price derived from the scale-up falls within the range of other carbon dioxide capture technologies.

As discussed in Section 2.4, fermentation was simulated at headspace pressures of 2 bar and 10 bar to identify the optimal configuration, with results detailed in Section 3.1. The fermenter accounts for the largest

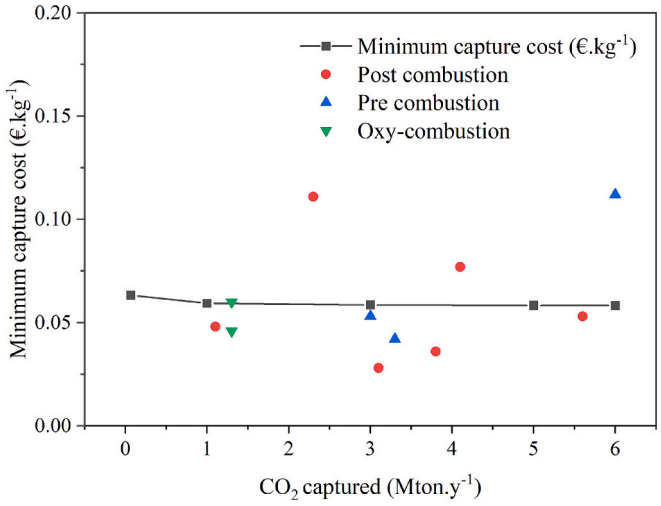


Fig. 9. Effect of plant size on the minimum CO_2 selling price (black squares). Also shown are CO_2 selling costs from the literature for different capture technologies: red dots for post-combustion, blue triangles for pre-combustion, and green triangles for oxy-combustion, across various scales.

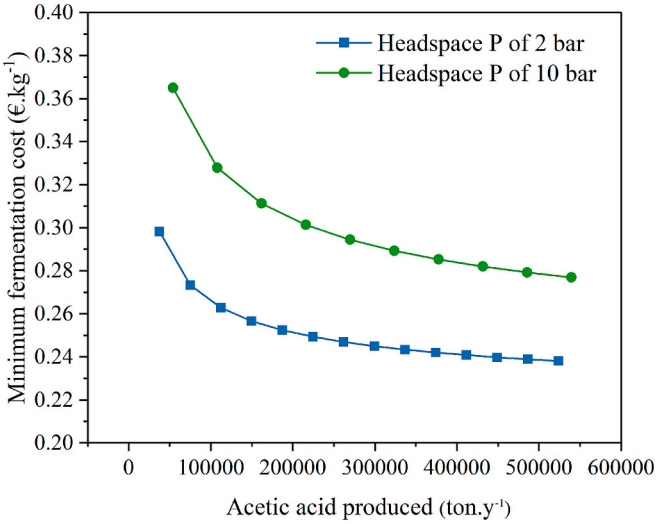


Fig. 10. Minimum gas fermentation cost as a function of plant size for processes with headspace pressures of 2 bar and 10 bar.

share of TEC for the fermentation section, representing 76.79 % at 2 bar and 69.41 % at 10 bar. This substantial share of the total capital expenditure underscores the critical influence of the reactor size (862 m^3). At 10 bar, the TPI more than doubles compared to 2 bar due to higher capital costs for the fermenter, compressors, and heaters. Additionally, higher pressure increases acetic acid production and reactant requirements, leading to greater PECs for shared equipment due to higher flow rates. Operational expenses are largely influenced by raw materials, including nutrients, water make-up, and bacterial inoculum, rather than utilities. Nutrients, essential for bacterial growth, account for nearly the entire raw material cost. Variable operating costs are slightly higher at 10 bar due to increased electricity and cold utility demand, though the impact is minor since raw materials represent the largest portion of these costs. Fixed operating costs are also higher at 10 bar due to increased labor needs for operating additional equipment. Section S12 of the Supplementary Materials provides details on the operational and capital costs for the fermentation process. The minimum fermentation cost, determined using the iterative procedure in Section 2.7.3 to achieve an NPV of 0, is 0.298 €.kg^{-1} at 2 bar headspace pressure and 0.365 €.kg^{-1} at 10 bar headspace pressure.

The capacities of pure acetic acid production from a single fermenter, as compared to Table S11.11 in Section S12, are small to medium relative to existing plants and gas fermentation studies, with a maximum of 180,000 ton.y^{-1}. In contrast, industrial acetic acid production from fossil sources can reach 500,000 ton.y^{-1}. To match this scale, the fermentation process was scaled up to 500,000 ton.y^{-1} by adding parallel fermenters, analyzing the impact on minimum cost. At 2 bar, 14 fermenters are required, while at 10 bar, only 10 are needed. Fig. 10 shows the minimum fermentation cost as a function of plant size. For capacities above 500,000 ton.y^{-1}, the minimum fermentation cost is 0.238 €.kg^{-1} at 2 bar and 0.277 €.kg^{-1} at 10 bar. Despite requiring fewer fermenters at 10 bar, the higher capital and operating costs associated with increased pressure result in higher fermentation costs. Therefore, subsequent steps (S-100 to S-800) were simulated using the operating conditions and results for fermentation at 2 bar headspace pressure. The electricity price is assumed to be 0.07 €.kWh^{-1}; however, an increase to 0.11–0.13 €.kWh^{-1} results in cost variations of less than 2.5 % of the fermentation cost.

The modelling of the purification section is described in Section 2.5, whereas the results of the simulation are presented in Section 3.1. The higher costs are mainly attributed to the azeotropic distillation columns (C-801), which contribute about 38 % of the total. Additionally, the filtration and ion exchange section (S-600) accounts for approximately 34 % due to the high flowrate requiring extensive resin use, which must be frequently replaced over the plant's lifetime. Details on the Total Project Investment and the percentage distribution of bare erected costs are available in Section S12 of the Supplementary Materials. Utilities account for 55.53 % of OPEX, driven by the high utility demand of the distillation columns, particularly the azeotropic column. Heating costs are the highest, due to medium-pressure steam consumption in the reboilers of C-801 and low-pressure steam use in the solvent recovery column (C-802). Cooling costs are also significant, owing to the condensers of multiple columns and numerous heat exchangers used to cool process streams. Raw materials contribute 33.52 % of OPEX, primarily due to the large solvent flowrate and the chemicals required for resin regeneration. Section S12 of the Supplementary Materials provides details on operating costs and the breakdown of variable costs per kilogram of acetic acid produced. The minimum selling price for the purification process was determined using the iterative procedure outlined in Section 2.7.3. For a plant producing 37 kton.y^{-1} of CH_3COOH, the total investment required is 33.95 M€, with annual fixed operating costs of 1.59 M€.y^{-1} and variable operating costs of 14.98 M€.y^{-1}. This results in a purification cost of 0.60 €.kg^{-1} of acetic acid produced. The electricity price is assumed to be 0.07 €.kWh^{-1}; however, an increase to 0.11–0.13 €.kWh^{-1} results in cost variations of less than 1 % per kilogram of acetic acid produced.

By combining costs from the Alkaline Electrolysis Section (S100), H_2S Removal Section (S200), CO_2 Capture Section (S300), O_2 Removal Section (S400), Fermentation Section (S500), Filtration and Ion Exchange Section (S600), Liquid-Liquid Extraction Section (S700), and Solvent, Acid, and Water Recovery Section (S800), a minimum acetic acid selling price of 1.575 €.kg^{-1} was calculated for a production rate of 37 kton.y^{-1} (electricity price assumed to be 0.07 €.kWh^{-1}). Individual contributions are detailed in Table 3.

The highest costs are observed in purification (37.8 % of the final price) and hydrogen production (36.4 %). Regarding capital expenditure, electrolysers are the costliest, contributing over 34 % of the TEC. Azeotropic columns and resins in the purification section add 14.54 % and 12.85 %, respectively, while the fermenter accounts for 11.93 %. The process analysis, detailed in Fig. 11, shows that utilities are the primary driver of OPEX, contributing over half of the total. Among utilities, hydrogen production is the largest cost component, with electricity consumption accounting for over 45 %. The purification phase follows, contributing 38 % due to high demand for hot (29.29 %) and cold (8.25 %) utilities. Additionally, amine regeneration in CO_2 capture

Table 3
Cost breakdown for hydrogen production, CO_2 capture, fermentation (at 2 bar headspace pressure), purification per kilogram of acetic acid, and the total price of acetic acid. Based on a plant productivity of 37 kton.y^{-1} in 2023 (electricity price assumed to be 0.07 €.kWh^{-1}).

ITEM	Price in 2023 (€.kg^{-1} of acetic acid)
H_2 (S-100)	0.573
CO_2 (S-200, S-300 and S-400)	0.108
Fermentation with a headspace pressure of 2 bar (S-500)	0.298
Purification (S-600, S-700 and S-800)	0.596
Entire process	1.575

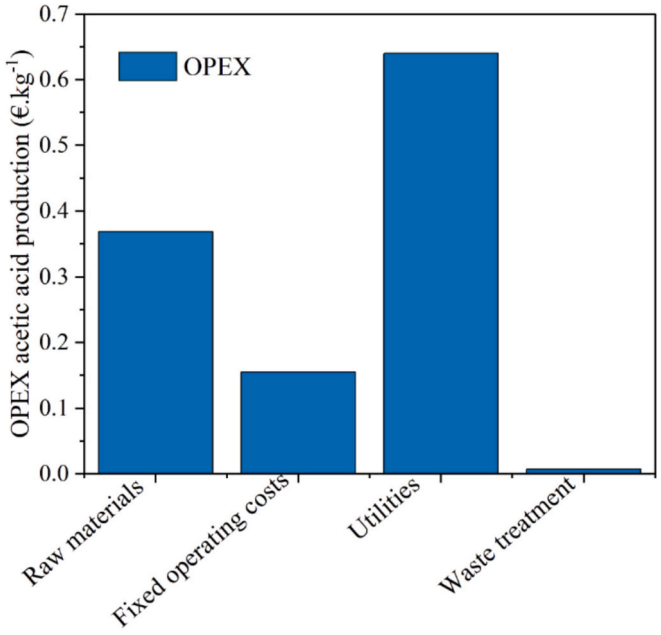


Fig. 11. Breakdown of operating expenses for acetic acid production at a plant with a productivity of 37 kton.y^{-1}.

represents 10.69 % of total utility costs. For raw materials, fermentation leads with nutrient costs exceeding 55 % of the total, while 40.3 % is attributed to purification, driven by resin regeneration chemicals and MTBE make-up. Fixed operating costs are significant due to the large equipment count and high TPI, while waste treatment costs remain low.

A scale-up analysis was conducted to assess how acetic acid price varies with plant size by adopting multiple parallel fermenters. CAPEX was estimated using Eq. (4), while OPEX, including wages, was scaled proportionally to productivity (with the electricity price assumed to be 0.07 €.kWh^{-1}). The largest scale considered aligns with upcoming green hydrogen projects, such as the HYSYNERGY project, targeting 20 kton.y^{-1} of hydrogen by 2025 [87]. This corresponds to using 4 fermenters, achieving a productivity of 150 kton.y^{-1} of acetic acid and requiring 20.49 kton.y^{-1} of hydrogen. Scaling further to match large methanol carbonylation plants for acetic acid production, as shown in Table S11.11 in Section S12 of the Supplementary Materials, would require up to 14 fermenters and 71.70 kton.y^{-1} of hydrogen, making it impractical with current or near-future hydrogen capacities. Nevertheless, this analysis highlights how production capacity affects the minimum selling price (MSP) of acetic acid. Larger scales result in lower prices due to non-linear increases in capital costs and fixed operating expenses. As the plant size increases, the MSP stabilizes and approaches a limit of approximately 1.17 €.kg^{-1}.

This scale-up was conducted to provide a first-order estimate of production costs at commercial scale and enable comparison with fossil-based market benchmarks. For capital-intensive units, such as electrolyzers, CO_2 absorption/stripping columns, fermenters, and purification sections (extraction and distillation), the scale-up was implemented by replicating identical units in parallel, rather than increasing unit size. This modular strategy, widely used in process industries, improves constructability, reduces engineering complexity, and enhances operational flexibility.

Replication of standardized equipment benefits from procurement efficiencies, standardization, and "learning-by-doing" effects, which reduce per-unit capital costs. This principle is supported by established cost exponent data for typical process equipment (γ = 0.44–0.60) [42,88,89] and substantiated by case studies in modular chemical plants showing capital cost trends consistent with the six-tenths rule [90].

The impact of projected hydrogen production costs for 2030 on acetic acid pricing was also evaluated. For a plant producing 37 kton.y^{-1} of acetic acid, the 2030 scenario shows a 14.62 % reduction in hydrogen production costs per kilogram of acetic acid, lowering the final price from 1.576 €.kg^{-1} to 1.492 €.kg^{-1}. In this case, purification accounts for 39.95 % of the final price, while hydrogen production contributes 32.80 %. Fig. 12 illustrates the trend of the minimum selling price of acetic acid as plant scale increases for both the 2023 and 2030 scenarios.

The comparison shows how the MSP of acetic acid for the 2030 scenario stabilizes in the largest scale at a price that is 5.20 % lower than the previous one, specifically 1.11 €.kg^{-1}. However, despite this drop at larger scales, the price remains significantly higher than the 2023 market value of GAA (0.6 €.kg^{-1} [91]).

Regarding the minimum acetic acid selling price in 2023, for a production rate of 37 kton.y^{-1}, it increases from 1.58 €.kg^{-1} to 1.80 €.kg^{-1} as the electricity price increases from 0.07 €.kWh^{-1} to 0.13 €.kWh^{-1}. For production rates above 500 kton.y^{-1}, the minimum acetic acid selling price rises from 1.17 €.kg^{-1} to 1.37 €.kg^{-1} under the same electricity price increase. The variation of the minimum acetic acid selling price in 2030 with respect to changes in electricity prices was also assessed. For a production rate of 37 kton.y^{-1}, the minimum acetic acid selling price increases from 1.49 €.kg^{-1} to 1.62 €.kg^{-1} when the electricity price rises from 0.07 €.kWh^{-1} to 0.11 €.kWh^{-1}. For production rates above 500 kton.y^{-1}, the minimum acetic acid selling price increases from 1.11 €.kg^{-1} to 1.22 €.kg^{-1} under the same electricity cost variation.

The process achieves a carbon efficiency of 78.54 %, meaning nearly 80 % of the carbon entering Section S-200 as CO_2 is effectively converted into acetic acid. This efficiency is achieved through recirculating

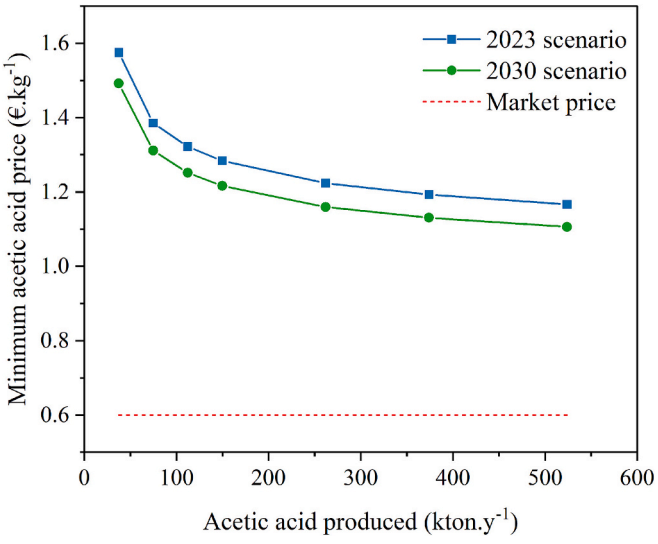


Fig. 12. Trend of the minimum acetic acid price as a function of plant size for the 2023 and 2030 scenarios, compared with the market price.

unreacted CO_2, high capture rates, and effective purification. If all carbon is converted into acetic acid, formic acid, biomass, and dissolved CO_2, the efficiency rises to 91.04 %.

3.3. Environmental analysis

The environmental assessment of 37 kton.y^{-1} of glacial bio-acetic acid produced using a process simulated with Aspen Plus® Version 10 and depicted in Fig. 1 (with details provided in Figs. 2–7 according to unit operations) was investigated through Life Cycle Assessment (LCA). LCA was performed with SimaPro 9.5 software and Ecoinvent 3.11 database, in agreement with ISO 14040-44:2006.

Table 4 presents the environmental impact calculated using the ReCiPe MidPoint (H) 2016 method, comparing the production of glacial bio-acetic acid and chemically produced glacial acetic acid. Table 4 also suggests process optimization based on identified hotspots and sensitivity analysis.

Based on the results shown in Table 4, it is noteworthy that the environmental impacts of glacial bio-acetic acid production were lower than those of chemically produced glacial acetic acid (based on the Ecoinvent 3.11 database). This outcome is particularly evident in impact categories related to climate change, fossil resource consumption, and water consumption, where the bio-based process largely outperformed the conventional chemical route.

To simplify the discussion of the results, the environmental impacts are considered normalised to 1 kg of glacial (bio- and chemical) acetic acid.

Focusing on climate change, the bio-based process resulted in 0.884 kg CO_2 eq.kg^{-1}, compared to 1.66 kg CO_2 eq.kg^{-1} for the traditional chemical process. These findings highlight that the use of biogenic CO_2, derived from the upgrading of biogas through anaerobic digestion (S-200), can effectively reduce climate change impact while producing a valuable product as glacial bio-acetic acid. This underscores the importance and effectiveness of carbon capture and utilization systems in achieving the decarbonization of production processes, as emphasized by the European Green Deal, which targets carbon neutrality by 2050.

(Miranda et al., 2023) investigated climate change impacts of the production of bio-based acetic acid through methanol hydrocarboxylation using CO_2 and H_2 as reagents, employing a bimetallic Ru—Rh homogeneous catalyst along with imidazole as a ligand and lithium iodide (LiI) as a promoter, with 1,3-dimethyl-2-imidazolidinone (DMI) as a solvent [29]. The LCA performed by (Miranda et al., 2023), considering a cradle-to-gate approach, is of 1.0 kg CO_2 eq.kg^{-1} of CH_3COOH [29]. The climate change impacts of our study were lower than those of (Miranda et al., 2023), due to the low amount of catalyst and the origin of CO_2 (derived from the biogas plant) and the biological nature of the process.

Fig. 13 presents the Sankey diagram for climate change, highlighting the main hotspots of the bio-based process: energy consumption and water consumption.

Energy consumption was further analyzed through the fossil resource scarcity impact category, where the bio-based process recorded 0.267 kg oil eq.kg^{-1}, compared to 0.997 kg oil eq.kg^{-1} for the traditional chemical process (a reduction of approximately 73 %). This significant decrease is a major advantage of bio-based processes, which typically rely on renewable biological resources rather than fossil-based raw materials, reducing dependence on non-renewable fossil fuels. However, the highest energy consumption was associated with units S-100, S-300, S-500, and S-700-800.

The hotspot related to energy requirement can be managed by

Table 4
Environmental impact calculated with the ReCiPe MidPoint (H) 2016 method. The environmental impacts refer to: 1) the production of glacial bio-acetic acid according to the FU 37 kton y^{-1}, and 2) normalised to 1 kg of bio-acetic acid (to simplify the visualisation of the data), 3) sensitivity analysis to show the effect of a 5 % bio-acetic acid reduction, 4) an optimized bio-acetic acid scenario with 50 % renewable biomass energy replacing fossil natural gas (Italian mix), since energy is a bottleneck of the process, and 5) comparative scenario for glacial acetic acid produced via a chemical route, utilizing Ecoinvent 3.11 data.

Impact category	Unit	Glacial bio-acetic acid production				Glacial-acetic acid production via a chemical route (as reference scenario)
		Based on FU	Normalised to 1 kg glacial bio-acetic acid	Sensitivity analysis	Optimized sceanrio. Normalised to 1 kg glacial bio-acetic acid	Normalised to 1 kg glacial acetic acid from Ecoinvent 3.11 database
Global warming	kg CO_2 eq	3.26E+07	8.84E-01	1.02E+00	5.12E-01	1.66E+00
Stratospheric ozone depletion	kg CFC11 eq	2.09E+01	5.66E-07	5.55E-07	4.22E-07	8.22E-07
Ionizing radiation	kBq Co-60 eq	4.03E+06	1.09E-01	9.15E-02	5.71E-02	1.20E-01
Ozone formation. Human health	kg NOx eq	5.55E+04	1.51E-03	2.26E-03	8.61E-04	4.15E-03
Fine particulate matter formation	kg PM2.5 eq	3.73E+04	1.01E-03	1.55E-03	6.34E-04	2.87E-03
Ozone formation. Terrestrial ecosystems	kg NOx eq	5.65E+04	1.53E-03	2.39E-03	8.77E-04	4.43E-03
Terrestrial acidification	kg SO_2 eq	1.10E+05	2.99E-03	3.62E-03	1.92E-03	6.06E-03
Freshwater eutrophication	kg P eq	8.83E+03	2.40E-04	4.07E-04	1.47E-04	7.79E-04
Marine eutrophication	kg N eq	7.89E+02	2.14E-05	2.22E-05	1.47E-05	3.41E-05
Terrestrial ecotoxicity	kg 1.4-DCB	5.50E+07	1.49E+00	3.16E+00	1.09E+00	6.41E+00
Freshwater ecotoxicity	kg 1.4-DCB	9.27E+05	2.51E-02	3.88E-02	1.64E-02	7.18E-02
Marine ecotoxicity	kg 1.4-DCB	1.21E+06	3.29E-02	5.12E-02	2.16E-02	9.51E-02
Human carcinogenic toxicity	kg 1.4-DCB	1.37E+06	3.71E-02	4.87E-02	2.69E-02	8.45E-02
Human non-carcinogenic toxicity	kg 1.4-DCB	1.87E+07	5.06E-01	8.00E-01	3.39E-01	1.49E+00
Land use	m^2a crop eq	8.82E+05	2.39E-02	3.01E-02	1.59E-02	5.12E-02
Mineral resource scarcity	kg Cu eq	6.11E+04	1.66E-03	2.70E-03	1.33E-03	5.09E-03
Fossil resource scarcity	kg oil eq	9.85E+06	2.67E-01	5.06E-01	1.44E-01	9.97E-01
Water consumption	m^3	6.23E+05	1.69E-02	2.44E-02	9.52E-03	4.40E-02

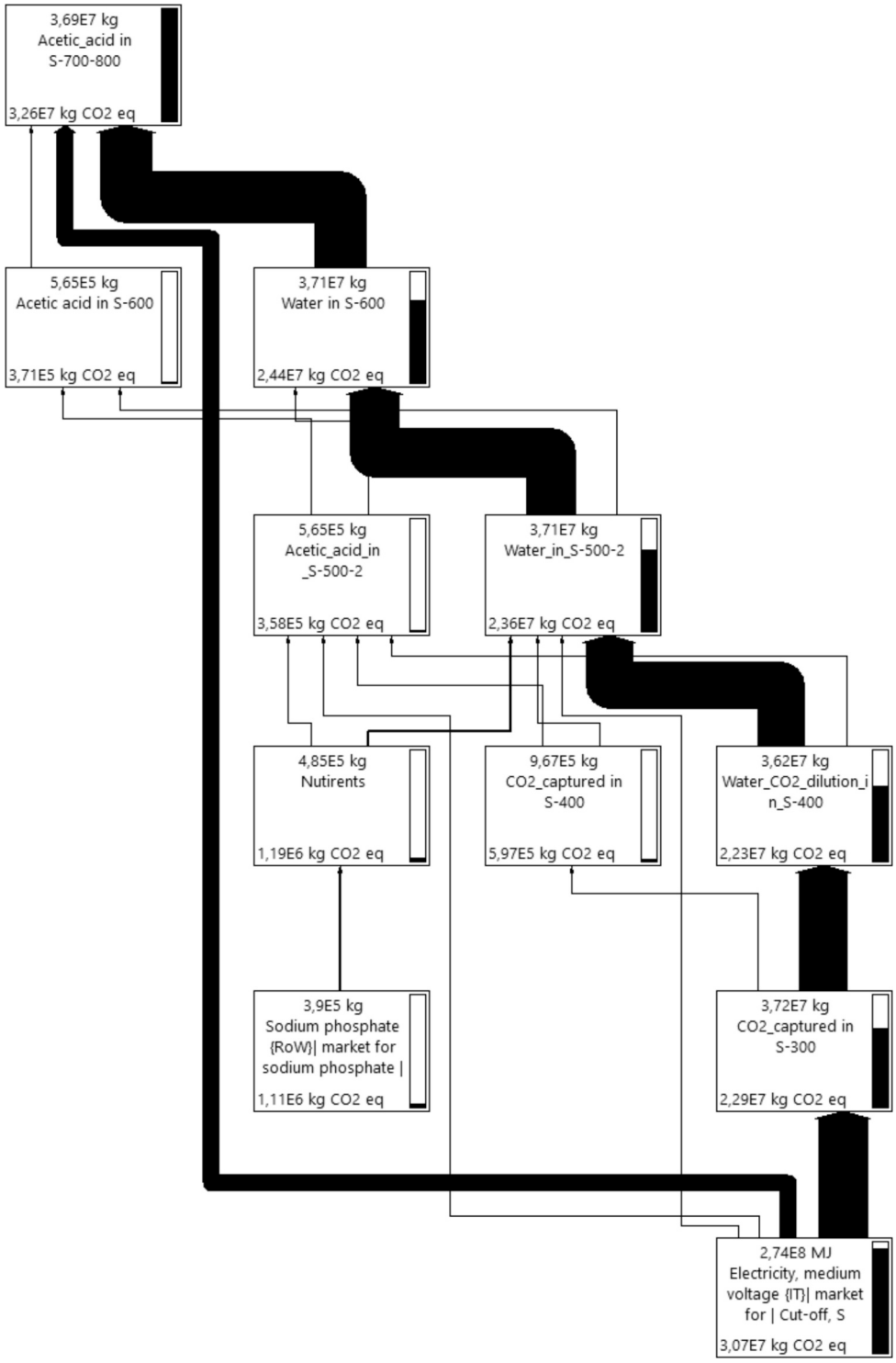


Fig. 13. Sankey diagram related to climate change impact category calculated with ReCiPe MidPoint (H) 2016. Result is based on FU.

integrating renewable energy, which can decrease carbon emissions and enhance energy efficiency. The National Renewable Energy Laboratory (NREL) projected that 100 % renewable electricity could be achieved by 2035, providing benefits that outweigh the related costs [92].

The bio-based process was modeled using the Italian energy mix. To optimize the process, Table 4 also presents a scenario where the energy mix consists of 50 % Italian grid electricity and 50 % biomass-based energy. This optimization can reduce climate change impact and fossil resource consumption by approximately 58 % and 54 %, respectively, proving effective. Biomass energy was chosen because it is a versatile renewable source that can produce heat, electricity, and biofuels. It is mainly generated through the conversion of organic waste, which also helps improve bio-waste management. Additionally, the decision was supported by data from the International Energy Agency (IEA, 2021), which states that in Italy (the focus area of this study), renewable energy must account for 55 % of gross final electricity consumption by 2030 [93]. Among renewable sources, biomass stands out as one of the most promising, since in 2019, there were 2946 bioenergy plants in Italy, with a total installed capacity of 4120 MW.

Regarding water consumption, the bio-based process used 0.0169

$m^3.kg^{-1}$, compared to 0.0440 $m^3.kg^{-1}$ for the traditional process (a reduction of about 61 %). This is a crucial advantage in terms of water conservation, particularly in regions facing water scarcity and considering water a limited resource. The water consumption impact reached in the present study was in line but slightly lower (about −5-7 %) than those identified in the study of (Marston et al., 2018) about 500 types of chemical industries [94].

The bio-based process also demonstrated lower human toxicity impacts, reducing carcinogenic and non-carcinogenic toxicity by approximately 56 % and 66 %, respectively. This suggests that biological materials may generate fewer harmful chemicals compared to conventional industrial processes.

Other notable environmental impacts include terrestrial acidification and eutrophication, both of which are relevant to bio-based processes due to the composition of growth media. The bio-based process showed around 50 % lower acidification potential (2.99E-03 vs. 6.06E-03 kg SO_2 eq.kg^{-1}), indicating a reduced contribution to soil acidification and acid rain formation. Currently, there are no available studies about glacial bio-acetic acid produced through gas fermentation. However, the terrestrial acidification and eutrophication results achieved in this study are lower than those of the study of Gadkari et al., 2021 performing electrochemical acetic acid production [95].

For eutrophication, the bio-based process generally performed better, showing lower eutrophication potential in both freshwater (2.40E-04 vs. 7.79E-04 kg P eq.kg^{-1}) and marine environments (2.14E-05 kg N eq.kg^{-1}).

The data consistency has been verified through a sensitivity analysis, which was conducted by reducing glacial bio-acetic acid production by 5 %. The results, reported in Table 4, confirmed the observed trends and demonstrated the robustness of the bio-based process in achieving lower environmental impacts compared to the chemical route.

Based on LCA data previously presented in the study, the impact of carbon pricing on the production cost of acetic acid was also assessed. In particular, the variation in the selling price of acetic acid under different carbon tax scenarios was evaluated for both the CO_2-based biotechnological process analyzed in this work and the conventional fossil-based production route. Regarding the CO_2-based fermentation process, the environmental impacts normalised to 1 kg of glacial acetic acid are the same for both the plant capacity analyzed in the LCA (37 kton.y^{-1}) and a larger-scale scenario (500 kton.y^{-1}). This is because OPEX was assumed to scale proportionally with the annual production volume of acetic acid. The selling prices of bio-based acetic acid at both production scales (37 kton.y^{-1} and 500 kton.y^{-1}) were compared with the conventional fossil-based process under carbon pricing scenarios ranging from 0 to 200 €.tonCO_2^{-1} [96].

This comparative analysis shows that the CO_2-based process becomes increasingly economically competitive with rising carbon prices, due to its significantly lower CO_2 emissions per kilogram of product (approximately half compared to the fossil-based route). At a carbon price of 100 €.tonCO_2^{-1}, the conventional process still yields a lower selling price, particularly at the 37 kton.y^{-1} scale. However, at 200 €.tonCO_2^{-1}, the gap between the fossil-based and bio-based acetic acid prices narrows considerably, especially for the larger-scale plant. Table 5 reports the selling price (€.kg^{-1}) of bio-based acetic acid at two production scales (37 kton.y^{-1} and 500 kton.y^{-1}) and of fossil-based acetic acid under increasing carbon tax scenarios (0–200 €.tonCO_2^{-1}).

Table 5
Effect of carbon pricing on the production cost of bio-based and fossil-based acetic acid.

Carbon pricing (€.ton^{-1})	Bio acetic acid (€.kg^{-1}) [Scale 37 kton.y^{-1}]	Bio acetic acid (€.kg-1) [Scale 500 kton.y-1]	Fossil fuel based acetic acid (€.kg-1)
0	1.58	1.17	0.60
50	1.62	1.21	0.68
100	1.66	1.25	0.77
150	1.71	1.30	0.85
200	1.75	1.34	0.93

4. Conclusions

Acetic acid is widely used in various industrial applications, and its synthesis via gas fermentation offers a promising alternative to traditional synthetic and sugar-based processes. However, to date, techno-economic studies have primarily focused on ethanol production via syngas fermentation, with limited attention to alternative platform chemicals such as acetic acid. No existing work comprehensively integrates CO_2 captured from biogas upgrading and hydrogen from alkaline electrolysis for the production of glacial bio-acetic acid. Furthermore, downstream separation of the highly diluted fermentation broth has not been thoroughly explored, nor has the influence of reactor pressure on productivity and by-product formation. This study addresses these gaps by presenting the first integrated simulation and techno-economic evaluation of bio-based glacial acetic acid (99.9 wt%) production through microbial fermentation, from gas feed to final purified product.

The gas fermentation process utilizes hydrogen from alkaline electrolysis and carbon dioxide captured via monoethanolamine absorption. These substrates are fed into a bioreactor, and since fermentation produces a highly diluted acetic acid solution, purification is performed using the HEDP process. The hydrogen produced has a purity of 80.17 wt %, with the water electrolysis plant sized for a productivity of 5.67 kton.y^{-1}. Carbon dioxide is captured from a biogas upgrading process (OFMSW to bio-methane) using chemical absorption with MEA. Before CO_2 capture, H_2S traces are removed, and after absorption, residual oxygen is eliminated. The capture process achieves at least 90 % CO_2 absorption, producing 70.97 kton.y^{-1} of 99.5 wt% CO_2. The vapor fraction, excluding CO_2 and H_2, is water. As fermentation occurs in an aqueous environment, high substrate purity is unnecessary, reducing production costs. The process simulation captures the complexity of fermentation through a bubble column reactor model operating at two different headspace pressures (2 and 10 bar), thereby highlighting key trade-offs between productivity, by-product formation, and downstream separation complexity. The results demonstrate that operating at 2 bar, acetic acid production costs were lower, despite reduced single-fermenter productivity. Additionally, negligible formic acid was formed, simplifying purification. A single bubble column at 2 bar produced 37 kton.y^{-1} of acetic acid at 1.5 wt% in the broth. To overcome limitations associated with conventional distillation a hybrid downstream separation strategy, combining solvent extraction with azeotropic distillation, was designed and implemented. This approach enables achieving 99.8 % recovery and 99.9 wt% purity, meeting GAA market standards. Energy consumption was minimized through optimized heat exchange between process streams.

An economic analysis was conducted to determine the MSP of acetic acid by evaluating total investment and operating costs. For hydrogen production, over 78 % of PEC is attributable to the electrolyzer, with electricity demand dominating OPEX. This results in a hydrogen price of 3.77 €.kg^{-1} for a plant size of 5.68 kton.y^{-1}, dropping to 3.17 €.kg^{-1} under projected 2030 values. For CO_2 capture, the absorber and stripper account for over 40 % of TEC, while hot utility demand for solvent regeneration is the main OPEX contributor. A plant capturing 64.02 kton.y^{-1} achieves a CO_2 cost of 0.063 €.kg^{-1}. In the fermentation section, the bubble column fermenter represents the largest capital expense, while bacterial growth nutrients dominate OPEX. At 2 bar headspace pressure, fermentation costs are 0.298 €.kg^{-1} for a 37 kton.y^{-1} plant, compared to 0.365 €.kg^{-1} at 10 bar for 53.94 kton.y^{-1}. Scaling up with multiple fermenters reveals lower costs at 2 bar, leading to its selection for operation. In the purification section, azeotropic distillation columns and ion exchange resins account for approximately 72 % of the TEC. Regarding OPEX, the largest contributors are the high hot utility demand for column reboilers and the significant consumption

of MTBE and chemicals for resin regeneration. For a productivity of 37 kton.y^{-1}, the acetic acid price is 1.58 €.kg^{-1}. A scale-up analysis showed the price stabilizing at approximately 1.17 €.kg^{-1} for larger, traditional-scale plants. Considering projected 2030 hydrogen production values, the price at scale drops further to 1.11 €.kg^{-1}, though this remains significantly higher than the 2023 market price of 0.6 €.kg^{-1}. Future work should aim to validate and refine this approach using updated industry benchmarks, detailed vendor cost data, and direct consultation with industrial partners to enhance the accuracy of capital cost estimates at commercial scale.

Despite economic limitations, the process offers key environmental advantages. Nearly 80 % of the carbon entering the capture section is converted to acetic acid, demonstrating a high degree of carbon utilization and potential for significant fossil carbon displacement. The Life Cycle Assessment proved that the bio-based glacial acetic acid process reached lower climate change, fossil resource consumption, water consumption, and toxicity impact than the chemical process, emphasizing carbon capture system, and proposing a possible optimisation of the process using renewable energy sources.

The acetic acid fermentation process presents several opportunities for improvement. Hydrogen production via electrolysis is a promising green alternative, but challenges remain, including reducing electrolyzer costs, improving efficiency, and ensuring renewable electricity use. Research is also exploring electrolysers that can use seawater, reducing reliance on freshwater. Future challenges in CO_2 absorption include developing new solvents that are non-toxic, non-corrosive, and require less energy for regeneration. Amino blends may offer a promising alternative to the traditional MEA. Optimizing the bacterial medium in fermentation could reduce costs. For purification, process intensification could help lower the high costs of azeotropic distillation columns. Acetic acid could be purified to an intermediate level using these columns, with final purity achieved through hydrophilic hollow fiber membranes. These membranes, with a high affinity for water, can reject organic acids like acetic acid and offer a high surface area for purifying large flowrates.

CRediT authorship contribution statement

Francesco Regis: Writing – review & editing, Writing – original draft, Methodology, Investigation, Data curation, Conceptualization. **Francesca Demichelis:** Writing – review & editing, Methodology, Investigation. **Alessandro Monteverde:** Supervision, Resources, Investigation. **Debora Fino:** Supervision, Resources.

Funding

This research did not receive any specific grant from funding agencies in the public, commercial, or not-for-profit sectors.

Declaration of competing interest

The authors declare that they have no known competing financial interests or personal relationships that could have appeared to influence the work reported in this paper.

Acknowledgement

The authors thank ACEA Pinerolese Industriale Spa for providing the gaseous stream composition from their biodigester located near Turin.

Appendix A. Supplementary data

Supplementary data to this article can be found online at https://doi.org/10.1016/j.cej.2025.166138.

Data availability

Data will be made available on request.

References

[1] J.L. Martín-Espejo, J. Gandara-Loe, J.A. Odriozola, T.R. Reina, L. Pastor-Pérez, Sustainable routes for acetic acid production: traditional processes vs a low-carbon, biogas-based strategy, Sci. Total Environ. 840 (2022), https://doi.org/10.1016/j.scitotenv.2022.156663.
[2] A.C. Dimian, A.A. Kiss, Enhancing the separation efficiency in acetic acid manufacturing by methanol Carbonylation, Chem. Eng. Technol. 44 (2021) 1792–1802, https://doi.org/10.1002/ceat.202100230.
[3] C. Le Berre, P. Serp, P. Kalck, G.P. Torrence, Acetic acid in Ullmann's encyclopedia of industrial chemistry, Wiley. Weinheim 10 (2011), 14356007.
[4] P. Pal, J. Nayak, Acetic acid production and purification: critical review towards process intensification, Sep. Purif. Rev. 46 (2017) 44–61, https://doi.org/10.1080/15422119.2016.1185017.
[5] A. Vidra, Á. Németh, Bio-produced acetic acid: a review, Period. Polytech. Chem. Eng. 62 (2018) 245–256, https://doi.org/10.3311/PPch.11004.
[6] F.M. Liew, M.E. Martin, R.C. Tappel, B.D. Heijstra, C. Mihalcea, M. Köpke, Gas fermentation-a flexible platform for commercial scale production of low-carbon-fuels and chemicals from waste and renewable feedstocks, Front. Microbiol. 7 (2016), https://doi.org/10.3389/fmicb.2016.00694.
[7] A.M. Henstra, J. Sipma, A. Rinzema, A.J. Stams, Microbiology of synthesis gas fermentation for biofuel production, Curr. Opin. Biotechnol. 18 (2007) 200–206, https://doi.org/10.1016/j.copbio.2007.03.008.
[8] S. Redl, M. Diender, T.Ø. Jensen, D.Z. Sousa, A.T. Nielsen, Exploiting the potential of gas fermentation, Ind. Crop. Prod. 106 (2017) 21–30, https://doi.org/10.1016/j.indcrop.2016.11.015.
[9] J. Gao, H.K. Atiyeh, J.R. Phillips, M.R. Wilkins, R.L. Huhnke, Development of low cost medium for ethanol production from syngas by Clostridium ragsdalei, Bioresour. Technol. 147 (2013) 508–515, https://doi.org/10.1016/j.biortech.2013.08.075.
[10] J.R. Phillips, R.L. Huhnke, H.K. Atiyeh, Syngas fermentation: a microbial conversion process of gaseous substrates to various products, Fermentation 3 (2017), https://doi.org/10.3390/fermentation3020028.
[11] V. Müller, New horizons in Acetogenic conversion of one-carbon substrates and biological hydrogen storage, Trends Biotechnol. 37 (2019) 1344–1354, https://doi.org/10.1016/j.tibtech.2019.05.008.
[12] F.P. Rosenbaum, V. Müller, *Moorella thermoacetica*: a promising cytochrome- and quinone-containing acetogenic bacterium as platform for a CO2-based bioeconomy, green Carbon 1 (2023) 2–13, https://doi.org/10.1016/j.greenca.2023.06.002.
[13] F. Regis, L. Tarraran, A. Monteverde, D. Fino, Screening of conditions for the acetic acid production from H2 and CO2 by Thermoanaerobacter kivui in a pressurized stirred tank bioreactor, Chem. Eng. J. 485 (2024) 149685, https://doi.org/10.1016/j.cej.2024.149685.
[14] Y.C. Ardila, J.E.J. Figueroa, B.H. Lunelli, R.M. Filho, M.R.W. Maciel, Simulation of ethanol production via fermentation of the synthesis gas using Aspen plustm, Chem. Eng. Trans. 37 (2014) 637–642, https://doi.org/10.3303/CET1437107.
[15] B. Sirigudi Rahul Rao, A.H. Johannes Karen High Sundar Madihally A Gordon Emslie, Biomass To Ethanol: Process Simulation, Validation And Sensitivity Analysis Of A Gasifier And A Bioreactor, n.d.
[16] J. Chen, J.A. Gomez, K. Höffner, P.I. Barton, M.A. Henson, Metabolic modeling of synthesis gas fermentation in bubble column reactors, Biotechnol. Biofuels 8 (2015) 1–12, https://doi.org/10.1186/s13068-015-0272-5.
[17] S. Michailos, D. Parker, C. Webb, Design, sustainability analysis and multiobjective optimisation of ethanol production via syngas fermentation, Waste Biomass Valoriz. 10 (2019) 865–876, https://doi.org/10.1007/s12649-017-0151-3.
[18] O. Pardo-Planas, H.K. Atiyeh, J.R. Phillips, C.P. Aichele, S. Mohammad, Process simulation of ethanol production from biomass gasification and syngas fermentation, Bioresour. Technol. 245 (2017) 925–932, https://doi.org/10.1016/j.biortech.2017.08.193.
[19] C. Piccolo, F. Bezzo, A techno-economic comparison between two technologies for bioethanol production from lignocellulose, Biomass Bioenergy 33 (2009) 478–491, https://doi.org/10.1016/j.biombioe.2008.08.008.
[20] F. Regis, A.H.A. Monteverde, D. Fino, A techno-economic assessment of bioethanol production from switchgrass through biomass gasification and syngas fermentation, Energy 274 (2023) 127318, https://doi.org/10.1016/j.energy.2023.127318.
[21] E.M. de Medeiros, H. Noorman, R. Maciel Filho, J.A. Posada, Production of ethanol fuel via syngas fermentation: optimization of economic performance and energy efficiency, Chem. Eng. Sci. X 5 (2020) 100056, https://doi.org/10.1016/j.cesx.2020.100056.
[22] R.M. Swanson, A. Platon, J.A. Satrio, R.C. Brown, Techno-Economic Analysis of Biomass-to-Liquids Production Based on Gasification Scenarios, ACS Natl. Meet. B, Abstr, 2009.
[23] B. Acharya, P. Roy, A. Dutta, Review of syngas fermentation processes for bioethanol, Biofuels 5 (2014) 551–564, https://doi.org/10.1080/17597269.2014.1002996.
[24] P. Roy, A. Dutta, B. Deen, Greenhouse gas emissions and production cost of ethanol produced from biosyngas fermentation process, Bioresour. Technol. 192 (2015) 185–191, https://doi.org/10.1016/j.biortech.2015.05.056.

[25] C. Piccolo, F. Bezzo, A techno-economic comparison between two technologies for bioethanol production from lignocellulose, Biomass Bioenergy 33 (2009) 478–491, https://doi.org/10.1016/j.biombioe.2008.08.008.
[26] R.M. Swanson, J.A. Satrio, R.C. Brown, A. Platon, D.D. Hsu, Techno-Economic Analysis of Biofuels Production Based on Gasification, 2010.
[27] E.M. de Medeiros, H. Noorman, R. Maciel Filho, J.A. Posada, Production of ethanol fuel via syngas fermentation: optimization of economic performance and energy efficiency, Chem. Eng. Sci. X 5 (2020) 100056, https://doi.org/10.1016/j.cesx.2020.100056.
[28] D. Choi, D.C. Chipman, S.C. Bents, R.C. Brown, A techno-economic analysis of polyhydroxyalkanoate and hydrogen production from syngas fermentation of gasified biomass, Appl. Biochem. Biotechnol. 160 (2010) 1032–1046, https://doi.org/10.1007/s12010-009-8560-9.
[29] D.S. da Miranda, L.P. Martins, B.A.S. de Teles, I.L.C. Cunha, N.A. de Menezes, H. Sakamoto, L. Kulay, Alternative integrated ethanol, urea, and acetic acid processing routes employing CCU: a prospective study through a life cycle perspective, Sustain 15 (2023), https://doi.org/10.3390/su152215937.
[30] F. Regis, Microbial CO2 Conversion to Acetic Acid: From Laboratory Testing to an Industrial-Scale Model, Politecnico di Torino, 2024.
[31] J. Holmgren, India: Potential for Developing Agricultural Residues to Sustainable Ethanol, (n.d.). https://www.indianchemicalnews.com/opinion/india-potential-for-developing-agricultural-residues-to-sustainable-ethanol-13316 (accessed April 21, 2024).
[32] CORDIS, Production of Sustainable, Advanced Bio-Ethanol through an Innovative Gas-Fermentation Process Using Exhaust Gases Emitted in the Steel Industry, (n.d.). https://cordis.europa.eu/project/id/656437 (accessed April 21, 2024).
[33] Y. Guo, G. Li, J. Zhou, Y. Liu, Comparison between hydrogen production by alkaline water electrolysis and hydrogen production by PEM electrolysis, IOP Conf. Ser. Earth Environ. Sci. 371 (2019), https://doi.org/10.1088/1755-1315/371/4/042022.
[34] A.Z. Arsad, M.A. Hannan, A.Q. Al-Shetwi, R.A. Begum, M.J. Hossain, P.J. Ker, T. I. Mahlia, Hydrogen electrolyser technologies and their modelling for sustainable energy production: a comprehensive review and suggestions, Int. J. Hydrogen Energy 48 (2023) 27841–27871, https://doi.org/10.1016/j.ijhydene.2023.04.014.
[35] M. Sánchez, E. Amores, D. Abad, L. Rodríguez, C. Clemente-Jul, Aspen plus model of an alkaline electrolysis system for hydrogen production, Int. J. Hydrogen Energy 45 (2020) 3916–3929, https://doi.org/10.1016/j.ijhydene.2019.12.027.
[36] Merichem Technologies, H2S Removal from Gas Streams, (n.d.). https://merichemtech.com/sulfur-recovery-with-lo-cat/?doing_wp_cron=1725191918.7372579574584960937500 (accessed February 15, 2025).
[37] A.S. Bhown, B.C. Freeman, Analysis and status of post-combustion carbon dioxide capture technologies, Environ. Sci. Technol. 45 (2011) 8624–8632, https://doi.org/10.1021/es104291d.
[38] B.R. Madeddu Claudio, Errico Massimiliano, CO2 Capture by Reactive Absorption-Stripping Modeling, Analysis and Design, 1st, 2019.
[39] T. Peppel, D. Seeburg, G. Fulda, M. Kraus, U. Trommler, U. Roland, S. Wohlrab, Methods for the trace oxygen removal from methane-Rich gas streams, Chem. Eng. Technol. 40 (2017) 153–161, https://doi.org/10.1002/ceat.201600171.
[40] J. Crater, C. Galleher, J. Lievense, Consultancy on Large-scale Submerged Aerobic Cultivation Process Design - Final Technical Report, 2017 https://www.nrel.gov/docs/fy17osti/67963.pdf.
[41] C. Chilev, F. Lamari, M. Dicko, E. Simeonov, C. Chilev, F. Lamari, M. Dicko, E. Simeonov, Investigation of Acetic Acid Dehydration by Various Methods to Cite This Version: HAL Id: hal-03369925, 2021.
[42] R. Turton, Analysis, Synthesis, and Design of Chemical Processes Fourth Edition, 2013.
[43] European Commission, Clean Hydrogen JU - SRIA Key Performance Indicators (KPIs), (n.d.). https://www.clean-hydrogen.europa.eu/knowledge-management/strategy-map-and-key-performance-indicators/clean-hydrogen-ju-sria-key-performance-indicators-kpis_en (accessed February 15, 2025).
[44] J.M. Bressanin, B.C. Klein, M.F. Chagas, M.D.B. Watanabe, I.L. de Mesquita Sampaio, A. Bonomi, E.R. de Morais, O. Cavalett, Techno-economic and environmental assessment of biomass gasification and Fischer-Tropsch synthesis integrated to sugarcane biorefineries, Energies 13 (17) (2020), https://doi.org/10.3390/en13174576.
[45] M. Hänchen, A. Stiel, Z.R. Jovanovic, A. Steinfeld, Thermally driven copper oxide redox cycle for the separation of oxygen from gases, Ind. Eng. Chem. Res. 51 (2012) 7013–7021, https://doi.org/10.1021/ie202474s.
[46] E. Alonso, F.R. Field, R.E. Kirchain, Platinum availability for future automotive technologies, Environ. Sci. Technol. 46 (2012) 12986–12993, https://doi.org/10.1021/es301110e.
[47] Business Analytiq, Potassium Hydroxide Price Index, (n.d.). https://businessanalytiq.com/procurementanalytics/index/potassium-hydroxide-price-index/ (accessed February 15, 2025).
[48] X. Ding, H. Chen, J. Li, T. Zhou, Comparative techno-economic analysis of CO2 capture processes using blended amines, Carbon Capture Sci. Technol. 9 (2023) 100136, https://doi.org/10.1016/j.ccst.2023.100136.
[49] Chemanalyst, Chemanalyst. n.d. https://www.chemanalyst.com/ (accessed February 10, 2025).
[50] IEA, Italy. 2025. https://www.iea.org/countries/italy/energy-mix (accessed July 6, 2025).
[51] EU, Report on Energy Prices and Costs in Europe, 2025 (2024).
[52] European Commission, Italian National Energy and Climate Plans (NECPs), 2023.
[53] F. ENI, The Italian Electricity Market in 2030 between NECPs and Reality, 2025 https://www.feem.it/publications/the-italian-electricity-market-in-2030-between-necps-and-reality-what-do-we-expect-from-italian-wholesale-electricity-prices-if-national-targets-are-not-reached/.
[54] F. Regis, A.H.A. Monteverde, D. Fino, A techno-economic assessment of bioethanol production from switchgrass through biomass gasification and syngas fermentation, Energy 274 (2023) 127318, https://doi.org/10.1016/j.energy.2023.127318.
[55] W. Short, D. Packey, T. Holt, A manual for the economic evaluation of energy efficiency and renewable energy technologies, Renew. Energy 95 (73) (1995) 73–81. NREL/TP-462-5173.
[56] E. Tito, G. Zoppi, G. Pipitone, E. Miliotti, A. Di Fraia, A.M. Rizzo, R. Pirone, D. Chiaramonti, S. Bensaid, Conceptual design and techno-economic assessment of coupled hydrothermal liquefaction and aqueous phase reforming of lignocellulosic residues, J. Environ. Chem. Eng. 11 (2023) 109076, https://doi.org/10.1016/j.jece.2022.109076.
[57] S. Dokhani, M. Assadi, B.G. Pollet, Techno-economic assessment of hydrogen production from seawater, Int. J. Hydrogen Energy 48 (2023) 9592–9608, https://doi.org/10.1016/j.ijhydene.2022.11.200.
[58] I. Thushari, J. Vicheanteab, D. Janjaroen, Material flow analysis and life cycle assessment of solid waste management in urban green areas, Thailand, Sustain. Environ. Res. 30 (2020), https://doi.org/10.1186/s42834-020-00057-5.
[59] R. Clift, A. Doig, G. Finnveden, The application of life cycle assessment to integrated solid waste management. Part 1 - methodology, Process Saf. Environ. Prot. 78 (2000) 279–287, https://doi.org/10.1205/095758200530790.
[60] J. Clavreul, D. Guyonnet, T.H. Christensen, Quantifying uncertainty in LCA-modelling of waste management systems, Waste Manag. 32 (2012) 2482–2495, https://doi.org/10.1016/j.wasman.2012.07.008.
[61] Y. Li, T. Zhang, J. Ma, X. Deng, J. Gu, F. Yang, M. Ouyang, Study the effect of lye flow rate, temperature, system pressure and different current density on energy consumption in catalyst test and 500W commercial alkaline water electrolysis, Mater. Today Phys. 22 (2022) 100606, https://doi.org/10.1016/j.mtphys.2022.100606.
[62] W. Sparber, W. Weiss, B. Sanner, L. Angelino, M. De Gregorio, N. Février, W. Haslinger, A. Kujbus, S. Landolina, G. Stryi-Hipp, W. Helden, Strategic Research and Innovation Agenda 2021–2027. https://www.clean-hydrogen.europa.eu/about-us/key-documents/strategic-research-and-innovation-agenda_en, 2022.
[63] International Energy Agency, Global Hydrogen Review 2022. https://www.iea.org/reports/global-hydrogen-review-2022, 2022.
[64] International renewable energy agency, Green hydrogen cost reduction: scaling up Electrolysers to meet the 1.5°C Climate Goal. https://ec.europa.eu/commission/presscorner/detail/en/ip_22_3131, 2020.
[65] International energy agency (IEA), Global Hydrogen Review 2024. www.iea.org, 2024.
[66] European Comission, REPowerEU: A Plan to Rapidly Reduce Dependence on Russian Fossil Fuels and Fast Forward the Green Transition, 2022.
[67] IEA, The future of hydrogen: seizing today's opportunities, Futur. Hydrog.. https://www.iea.org/reports/the-future-of-hydrogen, 2019.
[68] K. Zouhri, S.Y. Lee, Evaluation and optimization of the alkaline water electrolysis ohmic polarization: exergy study, Int. J. Hydrogen Energy 41 (2016) 7253–7263, https://doi.org/10.1016/j.ijhydene.2016.03.119.
[69] B. Lee, H. Chae, N.H. Choi, C. Moon, S. Moon, H. Lim, Economic evaluation with sensitivity and profitability analysis for hydrogen production from water electrolysis in Korea, Int. J. Hydrogen Energy 42 (2017) 6462–6471, https://doi.org/10.1016/j.ijhydene.2016.12.153.
[70] W. Kuckshinrichs, T. Ketelaer, J.C. Koj, Economic analysis of improved alkaline water electrolysis, Front. Energy Res. 5 (2017), https://doi.org/10.3389/fenrg.2017.00001.
[71] F. Barbir, PEM electrolysis for production of hydrogen from renewable energy sources, Sol. Energy 78 (2005) 661–669, https://doi.org/10.1016/j.solener.2004.09.003.
[72] A. Hassanpouryouzband, E. Joonaki, K. Edlmann, R.S. Haszeldine, Offshore geological storage of hydrogen: is this our best option to achieve net-zero? ACS Energy Lett. 6 (2021) 2181–2186, https://doi.org/10.1021/acsenergylett.1c00845.
[73] F. Dawood, M. Anda, G.M. Shafiullah, Hydrogen production for energy: an overview, Int. J. Hydrogen Energy 45 (2020) 3847–3869, https://doi.org/10.1016/j.ijhydene.2019.12.059.
[74] M.R. Shaner, H.A. Atwater, N.S. Lewis, E.W. McFarland, A comparative technoeconomic analysis of renewable hydrogen production using solar energy, Energ. Environ. Sci. 9 (2016) 2354–2371, https://doi.org/10.1039/c5ee02573g.
[75] J.L. Fan, P. Yu, K. Li, M. Xu, X. Zhang, A levelized cost of hydrogen (LCOH) comparison of coal-to-hydrogen with CCS and water electrolysis powered by renewable energy in China, Energy 242 (2022) 123003, https://doi.org/10.1016/j.energy.2021.123003.
[76] D. Jang, J. Kim, D. Kim, W.B. Han, S. Kang, Techno-economic analysis and Monte Carlo simulation of green hydrogen production technology through various water electrolysis technologies, Energ. Conver. Manage. 258 (2022) 115499, https://doi.org/10.1016/j.enconman.2022.115499.
[77] F. Vega, F.M. Baena-Moreno, L.M. Gallego Fernández, E. Portillo, B. Navarrete, Z. Zhang, Current status of CO2 chemical absorption research applied to CCS: towards full deployment at industrial scale, Appl. Energy 260 (2020) 114313, https://doi.org/10.1016/j.apenergy.2019.114313.
[78] E. Adu, Y. Li, Y. Zhang, Y. Xin, P. Tontiwachwuthikul, Optimization and energy assessment of technological process for CO2 capture system of natural gas and coal combustion, Energy Rep. 8 (2022) 7612–7627, https://doi.org/10.1016/j.egyr.2022.06.004.

[79] L.F. De Mello, R. Gobbo, G.T. Moure, I. Miracca, Oxy-combustion technology development for fluid catalytic crackers (FCC) - large pilot scale demonstration, Energy Procedia 37 (2013) 7815–7824, https://doi.org/10.1016/j.egypro.2013.06.562.
[80] E.S. Rubin, J.E. Davison, H.J. Herzog, The cost of CO2 capture and storage, Int. J. Greenh. Gas Control 40 (2015) 378–400, https://doi.org/10.1016/j.ijggc.2015.05.018.
[81] S. Yun, M.G. Jang, J.K. Kim, Techno-economic assessment and comparison of absorption and membrane CO2 capture processes for iron and steel industry, Energy 229 (2021) 120778, https://doi.org/10.1016/j.energy.2021.120778.
[82] H. Isogai, C.A. Myers, T. Nakagaki, Cost estimation of CCS integration into thermal power plants in Japan, Proc. Int. Conf. Power Eng. 9 (2021) 1–18, https://doi.org/10.1299/mej.22-00028.
[83] K. Damen, R. Faber, R. Gnutek, H.A.J. Van Dijk, C. Trapp, L. Valenz, Performance and modelling of the pre-combustion capture pilot plant at the Buggenum IGCC, Energy Procedia 63 (2014) 6207–6214, https://doi.org/10.1016/j.egypro.2014.11.652.
[84] M. Bailera, P. Lisbona, B. Peña, L.M. Romeo, A review on CO2mitigation in the iron and steel industry through power to X processes, J. CO2 Util. 46 (2021), https://doi.org/10.1016/j.jcou.2021.101456.
[85] Y. Yang, T. Du, Y. Li, Q. Yue, H. Wang, L. Liu, S. Che, Y. Wang, Techno-economic assessment and exergy analysis of iron and steel plant coupled MEA-CO2 capture process, J. Clean. Prod. 416 (2023) 137976, https://doi.org/10.1016/j.jclepro.2023.137976.
[86] M. Finkenrath, Cost and Performance of Carbon Dioxide Capture from Power Generation. https://www.iea.org/reports/cost-and-performance-of-carbon-dioxide-capture-from-power-generation, 2011.
[87] N. Muro-Suné, HySynergy Green H2 Production Plant, (n.d.). https://www.ramboll.com/projects/energy/hysynergy-green-h2-production-plant (accessed February 15, 2025).
[88] M.S. Peters, K.D. Timmerhaus, R.E. West, Plant Design and Economics for Chemical Engineers, 5th, 2003.
[89] Ulrich, G. D., Vasudevan, P. T. Chemical Engineering Process Design and Economics: A Practical Guide, 2nd ed. n.d.
[90] S. Lier, M. Grünewald, Net present value analysis of modular chemical production plants, Chem. Eng. Technol. 34 (2011) 809–816, https://doi.org/10.1002/ceat.201000380.
[91] Chemanalyst, Acetic Acid Price Trend and Forecast, (n.d.). https://www.chemanalyst.com/Pricing-data/acetic-acid-9 (accessed February 15, 2025).
[92] NREL, 100% Clean Electricity by 2035 Study, (n.d.). https://www.nrel.gov/analysis/100-percent-clean-electricity-by-2035-study.html (accessed March 9, 2025).
[93] International Energy Agency (IEA) Bioenergy, Implementation of bioenergy in Italy – 2021 update, 2021.
[94] L. Marston, Y. Ao, M. Konar, M.M. Mekonnen, A.Y. Hoekstra, High-resolution water footprints of production of the United States, Water Resour. Res. 54 (2018) 2288–2316, https://doi.org/10.1002/2017WR021923.
[95] S. Gadkari, B.H. Mirza Beigi, N. Aryal, J. Sadhukhan, Microbial electrosynthesis: is it sustainable for bioproduction of acetic acid? RSC Adv. 11 (2021) 9921–9932, https://doi.org/10.1039/d1ra00920f.
[96] IPCC, Climate Change 2022 - Mitigation of Climate Change - Full Report, 2022.